Ahmad Arslan

Comparative analysis of speed decoding algorithms for rotary incremental encoders

School of Electrical Engineering

Thesis submitted for examination for the degree of Master of Science in Technology.

Espoo 22.05.2017

Thesis supervisor:

Prof. Marko Hinkkanen

Thesis advisor:

Seppo Saarakkala, D.Sc. (Tech.)

Aalto University
School of Electrical Engineering

AALTO UNIVERSITY
SCHOOL OF ELECTRICAL ENGINEERING

ABSTRACT OF THE
MASTER'S THESIS

Author: Ahmad Arslan

Title: Comparative analysis of speed decoding algorithms for rotary incremental encoders

Date: 22.05.2017 Language: English Number of pages:5+49

Department of Electrical Engineering

Professorship: Electrical Drives Code: S-3016

Supervisor: Prof. Marko Hinkkanen

Advisor: Seppo Saarakkala, D.Sc. (Tech.)

Motion control process in modern automation technology and industry requires highly accurate speed information with high bandwidth. Incremental encoders are widely used as rotary feedback position and speed sensors which convert the motor position and speed information into coded electrical pulses. An accurate speed decoding system is therefore needed to extract necessary position and speed information from encoder output, which is further required by the motion control process. The level of accuracy and bandwidth highly depend on resolution of encoder being used as well as data processing technique. In this thesis, different incremental encoders and state-of-the-art speed decoding algorithms are discussed. These algorithms are implemented in Matlab Simulink and a comparative analysis is done based on accuracy, rapid response and wide speed range application. Further, the best choice is made based on this comparison and corresponding speed decoding algorithm is implemented in Xilinx FPGA. Analytical simulation results are presented in this thesis.

Keywords: Comparative analysis, Incremental encoder, rotary sensors, speed decoding algorithms

Preface

First of all, I would like to bow before ALLAH Almighty, the most Omnipotent, the most Merciful, the most Beneficial, Who bestowed me with such a lucid intelligence that I could endeavor my services towards this manuscript.

My first and foremost gratitude is for my beloved parents and siblings for their consistent support, love and sincere prayers. They always appreciated me and gave me the courage to achieve my goals and their colossal moral support has always been a source of inspiration for me.

It is my privilege and honor to express my gratitude to my research supervisor and mentor Prof. Marko Hinkkanen for his constructive supervision during the accomplishment of this thesis. I admire his patience, tenderness, devotion and intellectual supervision to spread knowledge and promote innovation. I have been amazingly fortunate to have an advisor who gave me the courage to explore on my own skills and affection to recover when my steps faltered. I would like to thank my thesis instructor Dr. Seppo Saarakkala for his continuous support. His office door was always open whenever I ran into a trouble spot or had a question about my research or writing. He consistently allowed this thesis to be my own work but steered me in the right direction whenever he thought I needed it.

Finally, I would like to thank all of my colleagues and friends at Electric Drives Research Group for creating a pleasent working environment and supporting me to accomplish my work.

Espoo, 22.05.2017

Ahmad Arslan

Contents

Symbols and abbreviations

Symbols

ω_m	Calculated angular speed
ω_r	Actual speed of the shaft
ω_{fm}	Calculated speed by frequency measurement method
ω_{pm}	Calculated speed by period measurement method
ω_{crit}	Critical speed
θ_g	Graduation angle (angular step)
$\Delta\theta_p$	Physical resolution
θ_{max}	Maximun covered angle
N_{pr}	Number of pulses per revolution
N	Number of (counted) pulses
ΔQ_ω	Quantization error
ε_{fm}	Relative error for frequency measurement method
ε_{pm}	Relative error for period measurement method
T_w	Time observation window (speed sampling time)
T_h	Time period of high frequency clock pulse
T_s	Sampling time
T_e	Incremental encoder pulse width
T_{eq}	New adopted time window for speed calculation
n	Number of periods of high frequency clock pulses

Abbreviations

ppr	Pulses per revolution
cpr	Counts per revolution
rpm	Revolution per minute
CCW	Counter clockwise
CW	Clockwise

1 Introduction

1.1 Background

Electric drives are the important components of modern automation technology and industry. Collectively as part of motion control systems, these devices are required to have capability of precise position, speed and torque control. A typical motion control system consists of a motor, a drive and a controller. The controller performs necessary calculations to obtain desired motion in result. To achieve high performance and accuracy, feedback devices such as encoders, play vital role by informing the controller or drive with details about actual position and movement of motor shaft.

Different types of rotary speed sensors are available in market based on technologies like magnetic, electromechanical, and optical. However, optical incremental encoders are widely used as speed sensors due to low maintenance, low cost and high noise immunity [1–5]. An optical incremental encoder contains a disc with a circular graduation track which consists of transparent and the non-transparent sequence of windows. These windows allow and restrict the optical beam from a source to reach the optical sensor periodically. Two fixed optical beam sources are placed on one side of the disc and are shifted, while sensors are located on the other side. When the shaft of an incremental encoder is rotated, it generates two electrical pulse trains which are shifted by quarter of the angular step of graduation. An angular step of graduation is the angular displacement starting from one non-transparent window to the end of successive transparent window. The shift between pulses is required to find the direction of rotation while the angular position of the encoder is directly proportional to the number of pulses produced [6], [7]. A third pulse is generated once in a complete (360°) revolution by another pair of optical beam source and sensor placed on a separate track with single transparent graduation. The pulse associated with this separate track provides the rotor position as reference. These output pulses carry low level information which are then fed to decoding circuitry in order to calculate shaft position as well as its speed which is further required for control purposes.

To calculate speed, a speed decoding system is required which should not only be compatible to the encoder being used, but should also be accurate, provide rapid response, and suitable for wide speed range [8]. Accuracy of speed measurement depends upon resolution of encoder which is governed by the structural design of graduation on the encoder disc. The design of encoder along with the data processing hardware or circuitry introduce quantization error in final measurement [9]. Therefore an estimation technique or some signal processing methods are required in order to minimize the quantization error and to obtain a measurement which should not deviate from actual value and should be suitable for all speed ranges.

Different speed calculation algorithms are presented in the literature with two basic approaches (frequency and period measurement method). The frequency measurement method is the one in which the number of electrical pulses from an encoder are counted inside a fixed time window. Because the number of pulses is directly proportional to the angular rotation of the shaft, the speed as well as angular position can easily be calculated [2], [3], [8], [10]. The frequency measurement method introduces quantization error especially at low speeds where pulse duration is too long, thus making it not suitable for the low speed region. The main advantage of this method is that a simple circuitry is required for its implementation and short time for processing, which makes it possible to produce good results at high speeds. Another basic technique is to measure the number of periods of high frequency clock pulse in one or more encoder pulses. This approach works better in low speed region, while at high speeds, when the encoder pulse may be smaller compared to high frequency clock period, the pulse interval is not measurable [11]. Moreover, this period measurement method also introduces quantization error, since it measures integer number of periods. The error is high at high speeds and provides accurate results in low speed region [2].

To be able to use both methods in the wide speed range, a combined technique based on both frequency and period measurement methods, is discussed in [2], [3], [8]. The switching between two methods is done by matching the error level produced by both methods in such a way, that above certain level of speed, estimation of speed is done by using the frequency measurement method. While below that level, the period measurement approach is used, thus reducing the quantization error to the acceptable limit. At very low speed, the combined method of frequency and period measurement is still not very suitable to be used. This is because of intermittent speed feedback to the controller due to the low frequency of the encoder pulses.

To overcome this situation, a variable combined method based on frequency and period measurement is presented in [5]. The traditional combined method of speed estimation based on frequency and period measurement method requires the fixed sampling period, while in variable method, the sampling time starts from the start of encoder pulse and ends with it. It has advantage in the low speed region, when the encoder pulse frequency is very low compared to sampling frequency, it turns to be period measurement method from start of one encoder pulse to its end, and produces the same relative error as in the period measurement method.

While at higher speeds, it combines the advantages of both frequency and period measurement approaches, since the relative error is almost same for both methods.

In [11], a new approach is proposed which uses the period measurement method. In this technique, unlike the traditional period measurement method, the average velocity measurement is synchronised with the timing of electrical pulses of encoders. It counts the number of pulses in the sampling time, the velocity is calculated but its value is not updated, until there is an alteration in the frequency of pulse train. The high accuracy of the period measurement method is further expanded to the high speed region by using this approach. The speed decoding time is fluctuant in this method. However, an additional processing circuitry is needed for detection of pulse alteration, which is a major disadvantage for this method.

To compensate for the quantization error, introduced due to lack of synchronization between the encoder pulse and the time observation interval, another approach is presented in [12, 13]. The time duration between bounds of the sample time interval and the incoming encoder pulse is measured. Based on this measured interval, a new time window is then assumed in such a way that the integer number of pulses falls inside this new window. This way, the quantization error can be reduced to zero. The main advantage of this method is that the same technique can be used for the wide speed range while no switching is required. The only quantization error which can be observed is due to digital counter used for time calculation.

1.2 Objectives

This thesis explores the cutting edge speed estimation algorithms targeting incremental encoders, subject to accuracy, rapid response time, wide speed range application and simple design structure. These algorithms are theoretically explained, implemented in Matlab Simulink and Xilinx FPGA and investigated by simulations and experiments. The main aim of this thesis is to analyse and compare each algorithm from its implementation to performance point of view and to highlight the main characteristics of each one. Filtering or signal conditioning methods are not considered.

1.3 Thesis structure

This thesis is divided into six sections. Section 2 explains the various rotary speed sensors and the design structure of optical incremental encoder in detail. Section 3 describes the design structure of different state-of-the-art speed decoding algorithms compatible with incremental encoders. In section 4, Matlab Simulink implementations of these algorithms are presented and a comparative analysis is made. Based on comparative analysis, implmenetation of one best algorithm in FPGA is discussed in section 5. Section 6 describes the overview of this thesis work and guides to further research work.

2 Incremental encoders

2.1 Rotary encoders: An overview

Rotary position and speed sensors are widely used for the purpose of performance monitoring and control in industrial processes and robotic manipulators. Rotary shaft encoders, however, are the transducers which are used for measuring the angular position and speed of rotating shaft [14]. Subject to application and environment, different types of encoders are available in the market. On the basis of the design structure and operating principle, there are three main types of position and speed feedback encoders 1) electromechanical, 2) incremental and 3) absolute encoders.

Tacho-generator and resolver are the two main types of electromechanical encoders used for rotary position and speed measurement. They convert the mechanical rotational information into analog electrical signals. A resolver [15–17] is basically a position feedback encoder with one rotor winding and two stator windings which are displaced by 90°. A signal of frequency typically from 6 to 8 kHz is fed to the rotor winding, and induced response signals are taken from the stator windings. The output, however, is the analog signal and usually needs to be converted in the digital form in order to be used by the modern micro-controller. The input signal to the rotary coil is fed through slip rings and brushes. The resolver, modulates the amplitude of the excitation signal on the rotor coil in proportion to the cosine and sine of the angle of mechanical rotation [15]. This electrical output signal in the form of sine and cosine wave received at stator windings carries the information about the position and speed.

The tacho-generator [17, 18], often called as DC tacho-generator, on the other hand, produces an analog voltage signal which is proportional to the rotational speed of the shaft. The polarity of the voltage depends on the direction of rotation. It works like a DC motor, with the magnetic field provided by permanent magnets. An electrical coil rotates in this magnetic field and produces an induced voltage which depends on both the speed as well as the direction of rotation. The voltage is then taken out through the brushes and the commutator for further signal processing. The output however, may contain ripples which may lead to oscillations in the

speed controller. A typical speed range for tacho-generators is up to 20,000 rpm, with output voltage up to 300 V and 0.5% to 10% ripple factor [16]. The speed range is, however, around 100,000 rpm in case of brush-less DC tacho-generator [18].

An incremental encoder is a rotary feedback position and speed transducer, which produces a coded (digital) output. The output is in the form of a pulse train, with the frequency in proportion to the rotational speed. It consists of a glass disk with graduation track(s) of transparent and non transparent windows of equal size. Digital signal output of incremental encoders increases or decreases with each incremental step of resolution. The signal generation and pick-off techniques used in the incremental encoder can be different. A detailed discussion about incremental encoders and signal generation is done in Section 2.2.

An absolute encoder, on the other hand [14–16], does not produce a pulse train for each step during shaft rotation. It generates a digital word in the form of binary code which identifies the accurate position of the shaft. The most common way to generate the coded output of the absolute encoder is through an optical method. In the optical method, light sources and photo-sensors are used with the coded disc of opaque and transparent regions. A coded disc gives information in the form of binary code as shown in Fig. 2.1. However, to avoid data interpretation problem [14] disc with gray coding can also be used. The absolute encoder provides accurate position

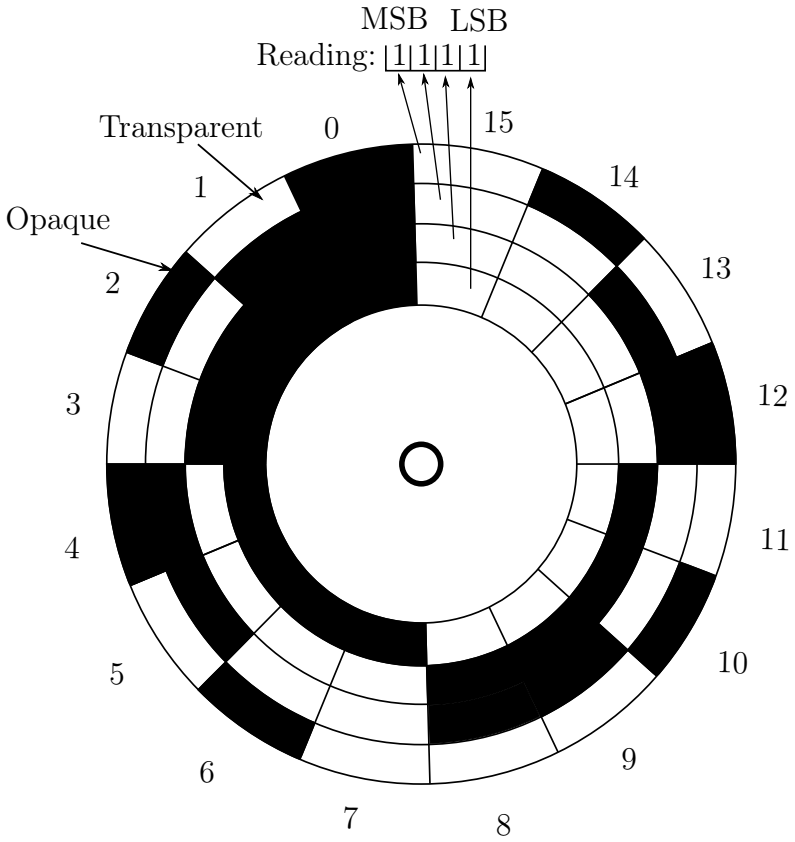

Figure 2.1: Absolute encoder coded disc.

of the shaft, even after the power outage, which an incremental encoder can not. An incremental encoder requires re-homing before starting the machine to rotate in order to provide position information. A typical absolute encoder available in the market can have a resolution of 4096 (12 bits) positions per revolution. More advance form of absolute encoders may be able to resolve 4,1941304 positions (22 bits) per revolutions [19]. An absolute encoder is commonly used to calculate the position of the shaft (fraction of revolution). However, it can also be used to measure multiple revolutions by introducing an additional track to produce the index pulse.

2.2 Incremental encoders

As discussed, an incremental encoder generates an output which is a digitally coded signal in the form of a pulse train. However, the design of an incremental encoder depends on the type of technology used to generate the output signal. Four kinds of mechanisms for signal generation and pick-off can be identified in the literature [14]. These methods of signal generation are also applicable in absolute encoders. Based on these technologies, incremental encoders can be further classified into four types (Fig. 2.2). These are further explained in more detail with their advantages and disadvantages.

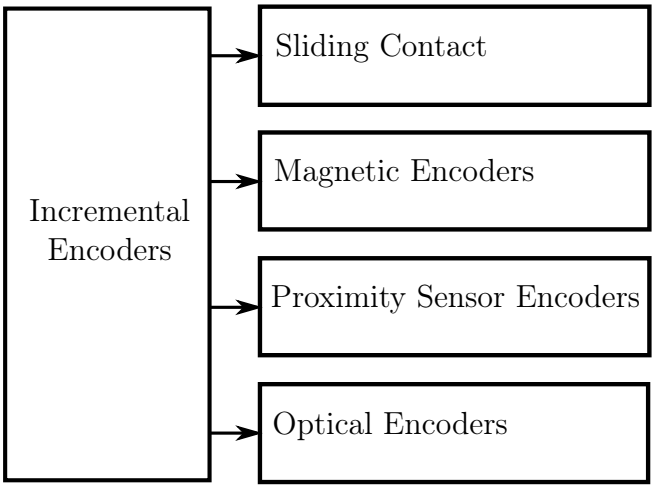

Figure 2.2: Classification of incremental encoders based on signal generation and pick-off method.

2.2.1 Sliding contact incremental encoders

An encoder with sliding contact mechanism consists of a disc made up of an electrically insulated material. The disc contains circular tracks with conducting and non-conducting areas. A slip ring is installed on the shaft of the encoder which is connected with all conducting areas on the circular tracks of the disc. A voltage of constant magnitude is applied to the conducting region of circular tracks

with the help of brushes sliding on the slip rings. To pick off the signal, a sliding contact is fixed in such a way, that it touches the circular path of the track (touching all conducting and non-conducting areas), as the disc rotates. The pattern of the generated pulse corresponds to the conducting and non-conducting regions of each track. It also depends upon the nature of rotation. The main advantages of incremental encoders with sliding contact mechanism include the simplicity of the design (economical) and the high sensitivity (proportional to the voltage). However, major disadvantages are because of the brush-slip ring commutation devices which includes, e.g., glitches in the signal, arcing, brush bounce [14].

2.2.2 Magnetic incremental encoders

In magnetic encoders, the encoder disc consists of magnetic and non magnetic regions imprinted on circular tracks on the disc [14, 20]. These magnetic regions are just like transparent areas in the glass disc of optical encoders. A micro-transformer is used to pick the signal. The sensors used to pick the signals are similar to the core storage elements in old technology computers. These sensors act as a transformer with primary and secondary windings. A schematic arrangement of a magnetic incremental encoder is shown in Fig. 2.3. The input voltage to the primary winding of micro-transformer (sensing element) is a high frequency (100 kHz) voltage signal. The induced voltage in the secondary has the same frequency. However, when magnetic spot on the disc approaches the sensing element, it saturates the core of the element. Which results in high reluctance and therefore decreases the induced voltage in the secondary. The output signal can be obtained by demodulating the

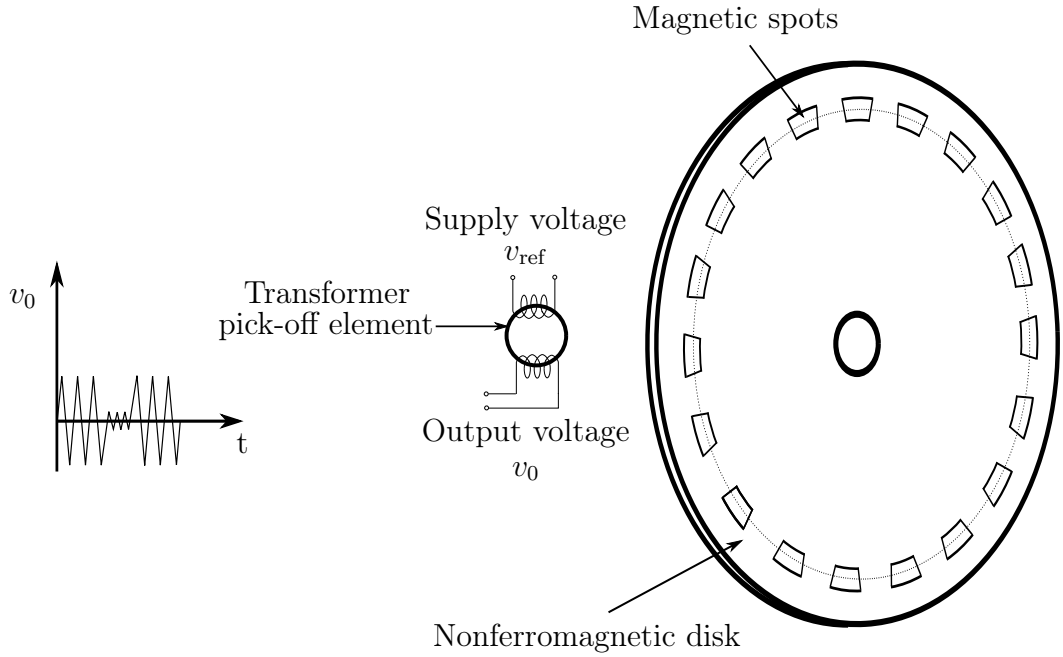

Figure 2.3: Magnetic incremental encoder schematic representation.

induced voltage. It is important to note that high peak in the pulse corresponds to the non-magnetic region between magnetic spots on the disk. However, to identify the direction of the magnetic field, sensors like hall effect and flux gate compasses can be used [21]. The contact-less signal pick-off method is the main advantage of this kind of encoder. However, these encoders are costly in comparison with sliding contact encoders, because of micro-transformer and circuitry to demodulate the induced voltage.

2.2.3 Proximity sensor incremental encoders

In proximity sensor incremental encoders [14], proximity sensors are used to sense the signal. Different proximity sensor elements such as eddy current probe or magnetic induction probe are used to pick-off the signal from rotating disk. However, magnetic induction probes are the most common choice. The encoder disk is now made of ferromagnetic material with raised spots on tracks. The material for these raised spots is the same as that of disk. The ferromagnetic toothed disk may also be used with radially placed proximity sensors as shown in Fig. 2.4. With the toothed disk, an encoder behaves like digital tachometer [14].

Now, as the raised area or the tooth of the disk approaches the probe, it increases the flux linkage and reduces the reluctance. A decrease in reluctance results in increased induced voltage. The output is again a modulated signal like in magnetic encoders and requires demodulating devices for further interpretation. The probes

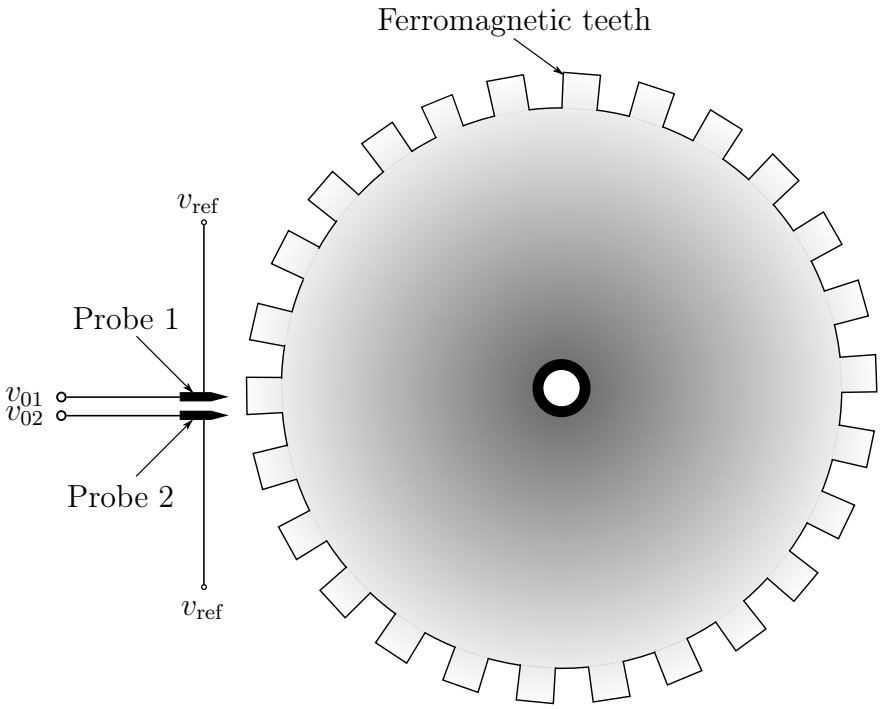

Figure 2.4: Proximity sensor incremental encoder disk configuration.

are placed in such a manner, that the output signals are shifted by 90°, required to identify the direction of rotation.

2.2.4 Optical incremental encoders

As the name suggests, an optical incremental encoder [1, 6, 7, 14], usually consists of a pair of light sources and light sensors for signal generation and pick off mechanism. It provides information about the rotor position and speed in the form of electrical pulses as the motor shaft is rotated. A disk with circular graduation tracks as a periodic sequence of transparent and non transparent windows is mounted on the shaft inside the encoder. The pairs of light sources and sensors are fixed along the tracks, in order to generate and sense the modulated signal. The contactless mechanism of signal generation and pick off with the simple configuration is the main advantages of an optical incremental encoder. These encoders are more reliable in comparison with previously explained and are the most common choice for industrial applications. However, absolute optical encoders are used over incremental encoders, where high accuracy is needed. A detailed discussion about the optical incremental encoder configuration and operation is presented in Section 2.3.

2.3 Operating principle

Optical incremental encoders are the most common choice for angular position and speed calculation within electric drives or at the shaft of a wheel. This is because of the low cost, low maintenance, and high noise immunity. However, signal interpretation may be the same for different types of incremental encoders used in industry. We may now limit our further discussion to optical incremental encoders.

Two possible configurations of an optical incremental encoder disk can be found in [14]:

1. Offset sensor configuration
2. Offset track configuration

In the offset sensor configuration, the encoder disk has a single circular track of equally spaced opaque and transparent windows. The area of transparent window is equal to the opaque area (space between two transparent windows). For the reference pulse signal, a track with a single transparent window is also introduced. This pulse is generated once in a complete revolution. A schematic diagram is shown in Fig. 2.5. Two pairs of light sources and sensors are fixed along the main track at quarter pitch. The pitch is center to center distance between two consecutive windows. Another pair of light source and sensor is fixed to generate and sense the pulse from the index window. It is important to notice that each pulse signal from the main track is on for half of the time period and off for the next half. Thus a continuous pulse train is generated as the disc rotates.

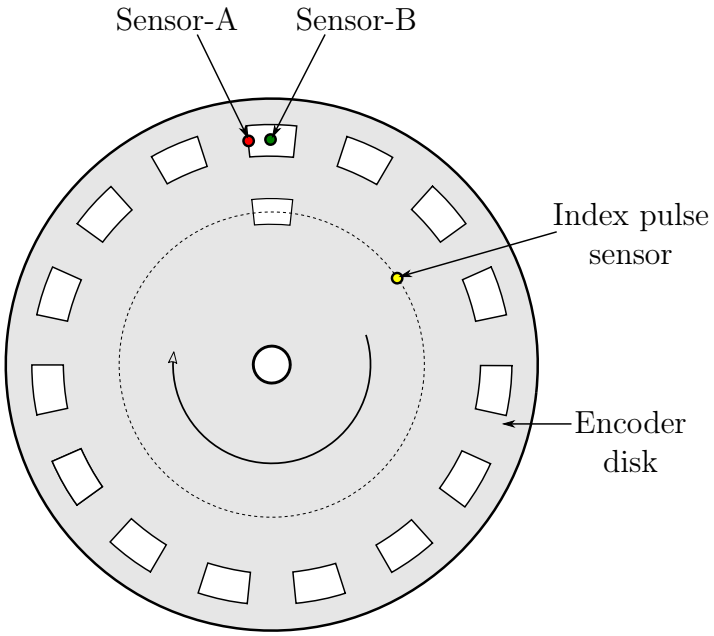

Figure 2.5: Offset sensor configuration.

A problem arises to fix sensors at quarter pitch distance along the graduation track of the encoder disc, since there is not enough space. One solution is to introduce an offset of integer number of periods between two sensing elements [14]. The delay between two signals is now an integer multiple of 360°, which can be easily interpreted.

In the offset track configuration as shown in Fig. 2.6, there are two separate

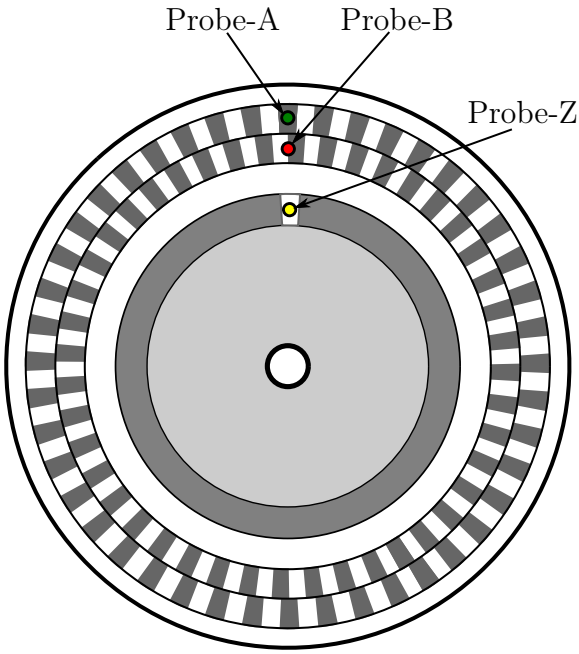

Figure 2.6: Offset track configuration.

identical tracks, one is displaced from other by a quarter pitch. A separate track with a single transparent window is introduced for the index pulse similar like in previous type.

When the shaft of the encoder is rotated, the disk also rotates, and the sensor corresponding to source A and B generates two separate pulse trains. Each pulse covers an angle equal to the angular step of graduation θ_p. A graduation angle is the one covered by a distance of one successive transparent and non-transparent window in the graduation track. The final angle θ, by which the disk is rotated is always an integer multiple of θ_g. Because the light sources along the main track are fixed by an offset equal to quarter of θ_g, the signals A and B are also shifted by the same angle ($\theta_g/4$). There are four switching events in the output pulses due to this shift. The offset between two pulses provides information about the direction of rotation. The construction principle for an optical incremental encoder with the offset sensor configuration is shown in Fig. 2.7. For the reference position, a separate index pulse (by LED-Z and corresponding sensor) is generated, once in a complete revolution (360°). The angle θ, corresponding to counter clockwise (CCW) direction is usually considered positive, while negative for clockwise (CW) rotation [6].

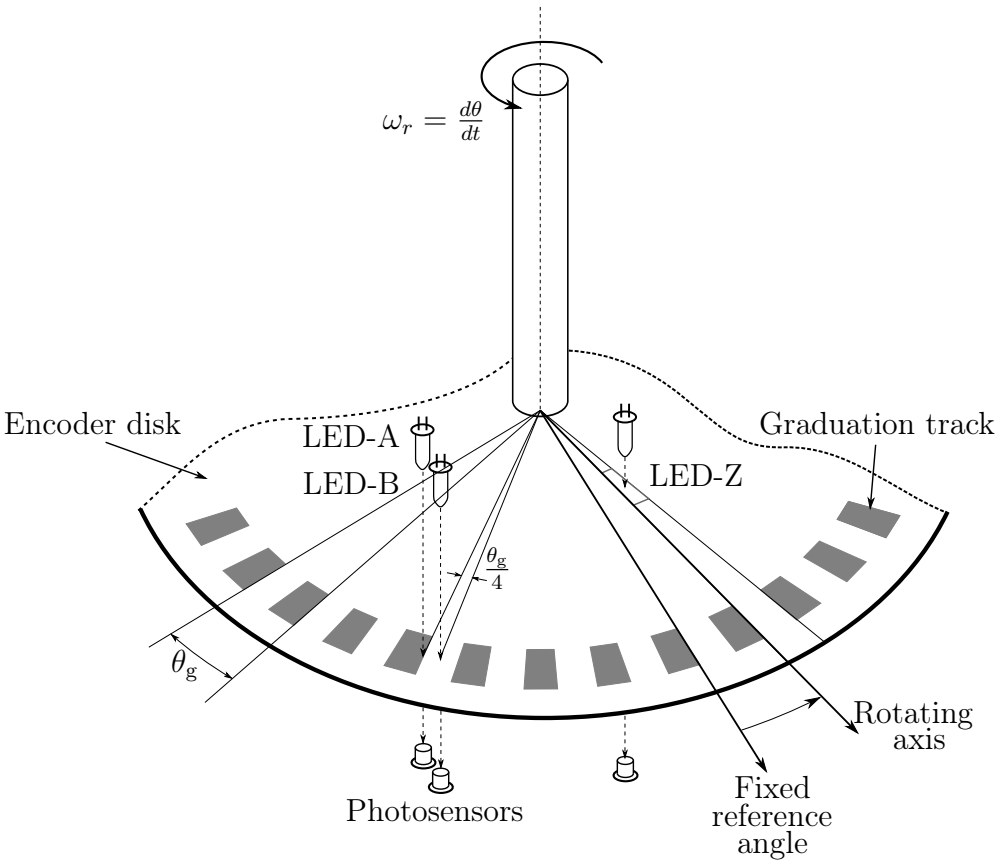

Figure 2.7: Optical incremental encoder: operating principle with offset sensor configuration.

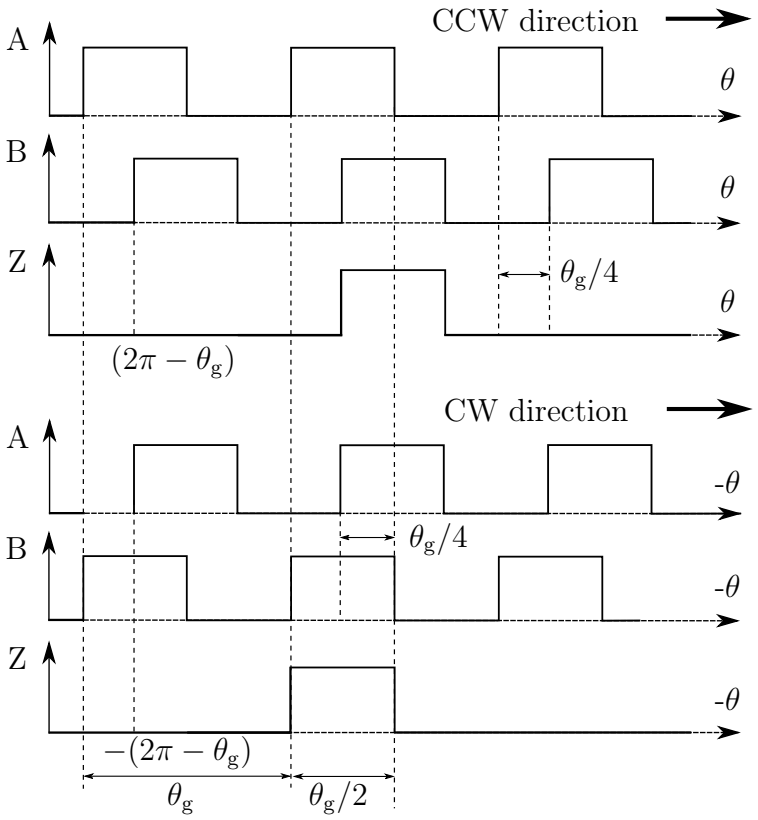

Figure 2.8: Output pulses for counter clockwise (CCW) and clockwise direction of rotation.

The output pulses (conditioned signals from all the three photo-sensors) are shown in Fig. 2.8. It can be noticed that during counter clockwise rotation (as shown in Fig. 2.7), the pulse A leads the pulse B by an angle of $\theta_g/4$. During the clockwise direction, it is vice versa. However, the index pulse (reference signal) comes once in one complete revolution. In reality these pulses are not ideal in shape.

Optical incremental encoders generally have very fine resolution compared to absolute encoders in a given technology. The magnetic scales are bit unsmooth compared to the optical scales. It is because the glass is the key component in fabricating high-resolution optical scales. The applications of optical incremental encoders may include the control robotics, process machinary feedback and measuring equipments. Often, the implementation of zeroing function is required in these applications when the machine is turned on. Additional rezeroing cycles can also be used in order to avoid error in position measurement which can be corrupted due to noise [20].

Different environmental parameters affect the performance of an optical incremental encoder. These include vibrations, shaft speed, frequency, temprature and supply voltage. The position as well as the speed is directly proportional to the frequency of output pulse signals. Fig. 2.9 shows the output frequencies of the incremental encoders of different resolutions, as a function of speed [18].

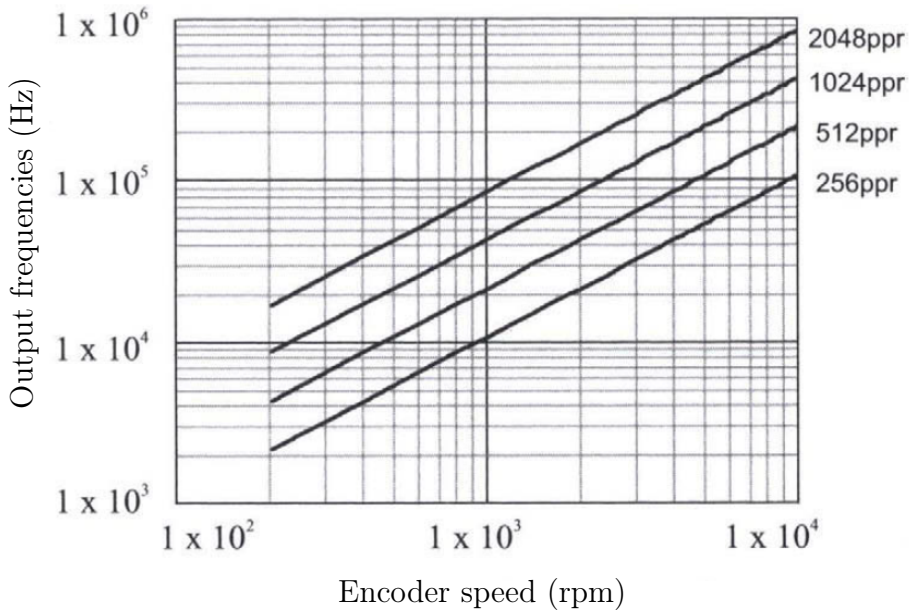

Figure 2.9: Encoder output frequency as function of speed for a range of incremental encoders [18].

The dimentions of a standard optical incremental encoder of 861xxxxxx series by *Leine & Linde* [22], is shown in Fig. 2.10. This is a six channel standard incremental encoder (RS422-supply 9-30 Vdc, output 5 Vdc) specifically designed for 12mm diameter hollow shaft with insulation. The resolution of this particular encoder is 2048 ppr with the maximum output fequency of 200 kHz. Encoders with resolution from 10 to 10000 ppr manufactured by the same company are available in market.

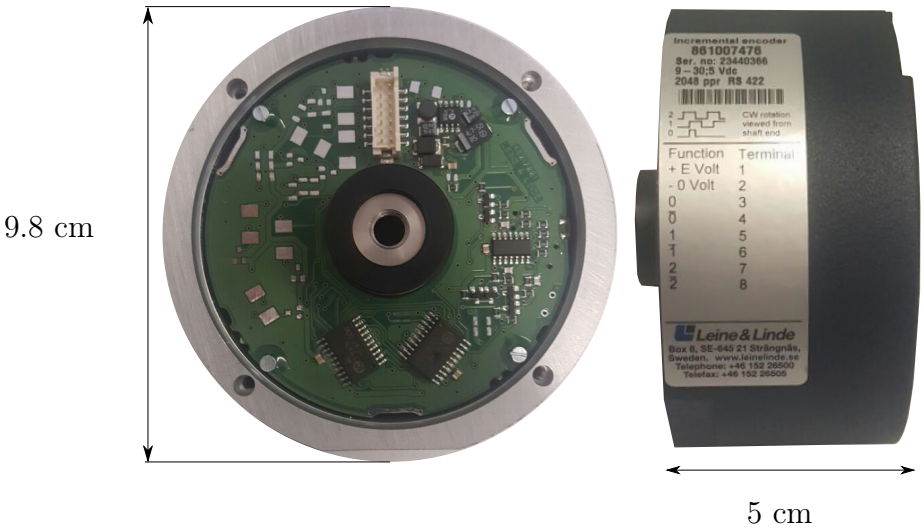

Figure 2.10: The dimentions of a standard optical incremental encoder of 861xxxxxx series by *Leine & Linde*.

2.3.1 Physical resolution

The resolution of an optical incremental encoder is decided by the number of pulses per revolution. The more the pulses per revolution the more would be the resolution. However, the factors, for example, the space for photo-sensors, and signal pick off at very high speeds, limit the size of transparent window, and thus the resolution.

Considering the detection of each rising edge in one complete revolution of the coded disk, the resolution (physical) is presented as the pitch angle $360°/N_{pr}$, where N_{pr} is the total counted rising edges. Since there are two pulses with an offset from one another by 1/4 of the pitch angle, one can also detect each rising and falling edge in both output pulses. Hence, the resolution can now be further increased by a factor of four, given as [14]

$$\Delta\theta_p = \frac{\theta_{max}}{4N_{pr}} \tag{2.1}$$

where θ_{max} represents the maximum angle covered by rotation of the disk. It is assumed to be equal to 2π (one complete revolution) in order to calculate the physical resolution of an incremental encoder. $\Delta\theta_p$ is the physical resolution which is inversely proportional to the number of pulses per revolution.

Each output signal of an incremental encoder has a resolution of half of the pitch, considering that all the transitions (rising and falling edges) are counted instead of counting pulses. According to this logic, for an encoder with 10,000 pulses per revolution, the resolution will be 0.018° when only one pulse is used (and two transitions in single pulse, both rising and falling edges are detected). If both the pulses are used simaltaneously, four transitions are then detected during a pitch cycle and therefore the resolution increases to 0.009° (2.1).

A summary of maximum resolution for various encoder types by *Dynaper Industry* [19], is presented in the Table. 2.1. Encoders with higher resolution are also available in the market. The physical resolution of an optical incremental encoder directly depends on its mechanical structure. That means no separate interpolation is involved. However, in order to detect and count the transitions, the output pulses should be ideal and perfect. The ideal shape can not be realized if the generated pulses are noisy. Thus the signal conditioning circuitry is necessary in order to shape the generated pulses.

Table 2.1: Summary chart of resolution for various encoder types [19].

Device	Resolution
Optical Incremental	10,000 ppr
Magnetic Incremental	2048 ppr
Optical Absolute	2^{22} cpr
Magnetic Absolute	4096 cpr

3 Speed decoding algorithms

This section encloses the discussion about various speed decoding algorithms. The required criteria for calculating the speed from the incremental encoder pulses are also explained, which are further required for comparison. A method to detect the direction of rotation is presented since it is being used by all the algorithms.

3.1 Requirement criteria

A speed controller often requires direct speed information from the motor for control purposes. Considering an optical incremental encoder as feedback sensor, a speed decoding system should fulfill certain requirements in order to facilitate the controller for precise control, for example:

1. A system to extract speed information from encoded signal provided by a rotary speed sensor should be highly accurate. Accuracy is the deviation of measured value from the actual. For control purposes, it is important to have accurate speed information.

2. It is difficult to detect the instantaneous change in speed using an incremental encoder, however an average of speed information can be calculated during a short time period. If the time window is extended, the realization of rapid speed response becomes difficult. It is because the lag time is also increased in the control system. Therefore, a speed measurement system should not only be accurate but also be able to provide information without significant computational delay.

3. A good speed decoding algorithm is the one, which is able to provide a highly accurate speed information during a very short observation time window. However, it should also be applicable to a wide speed range. Though, various algorithms are presented in the literature, but only a few can provide good results in wide speed range applications.

4. A good speed decoding method should be as simple as possible for its implementation. Although one can compromise over this considering the previous characteristics important. The complexity can increase the lag time to process the information.

3.2 Detection of rotation reversal

As presented in the Section 2.3, the output of an optical incremental encoder consists of quadrature pulses (A and B), which are 90° shifted from each other as shown in Fig. 2.8. The shift in these two pulses is provided in order to detect the change in direction of rotation. By comparing the relative position of both pulses, one can easily detect the change in direction of rotation. In Table 3.1, all the four possible combinations are presented for the detection of the rotation reversal. Further to this logic, an SR flip-flop with output Q & $\overline{\text{Q}}$ is required to further clarify the rotation direction. It should be noted that in Table 3.1, $0 \rightarrow 1$ represents the rising edge while, $1 \rightarrow 0$ denotes the falling edge for the corresponding logic variable. By this combinational logic, the change in direction can be detected during an increment of angle $\theta_g/4$.

The implementation is done by sampling of output logic A at every rising edge of B. As a result, the logic value will be 1 for anticlockwise (CCW) direction, and 0 for clockwise (CW) rotation. A block diagram structure for detection of the rotation reversal is shown in Fig. 3.1. The output of the SR flip-flop Q=1 only, when S=1 and becomes zero only when R=0 (CW signal), thus provides exact reversal information for a speed controlling subsystem.

Table 3.1: Signal combination to identify direction of rotation [7].

Rotation reversal detection			
CCW to CW ($Q = 1 \rightarrow Q = 0$)		CW to CCW ($Q = 0 \rightarrow Q = 1$)	
Triggered by R, if		Triggered by S, if	
A	**B**	**A**	**B**
0	$0 \rightarrow 1$	$0 \rightarrow 1$	0
$0 \rightarrow 1$	1	0	$1 \rightarrow 0$
$1 \rightarrow 0$	0	1	$0 \rightarrow 1$
1	$1 \rightarrow 0$	$1 \rightarrow 0$	1

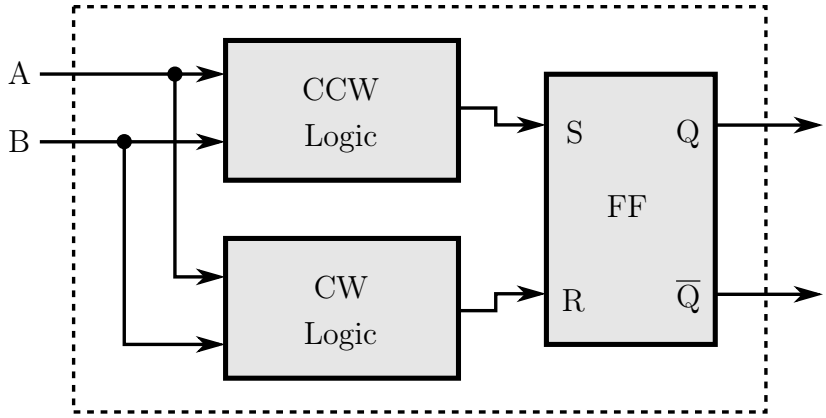

Figure 3.1: Block diagram representation for the detection of rotation reversal.

3.3 Angular position decoding algorithm

To calculate the speed, all the speed decoding algorithms are required to calculate the angular position θ with respect to the fixed reference axis (θ=0) [7]. The rotational speed is then computed by formula given as

$$\omega_m = \frac{\Delta\theta}{\Delta T_w} \tag{3.1}$$

where ω_m is the measured speed and T_w is the time observation window during which the speed is computed. Considering an optical incremental encoder, the angular position of the rotor shaft is estimated by counting the number of pulses generated by the incremental encoder. The counted value for the pulses is then multiplied with graduation angle θ_g. It is expressed mathematically as follows

$$\theta = \left(\overbrace{\sum N_a}^{\text{CCW}} - \overbrace{\sum N_b}^{\text{CW}} \right) \theta_g = \theta_g N \tag{3.2}$$

where N denotes to the number of counted pulses. To calculate the algebraic number of counted pulses, the direction of rotation is required. One can easily extract speed information from the angular position of the shaft. A block diagram representation of the angular position calculation method is shown in Fig. 3.2.

Two separate up-counters are used in order to count the number of pulses from encoder output terminals. Each of the two counters is dedicated to its own direction of rotation. The signal from the SR flip-flop is required to enable or disable the counter as the direction changes. An index pulse Z is used to reset each counter at the same time. The difference between pulse counts during counter clockwise and clockwise direction of rotation is then multiplied with the graduation angle (3.2) to get the position of the rotating shaft.

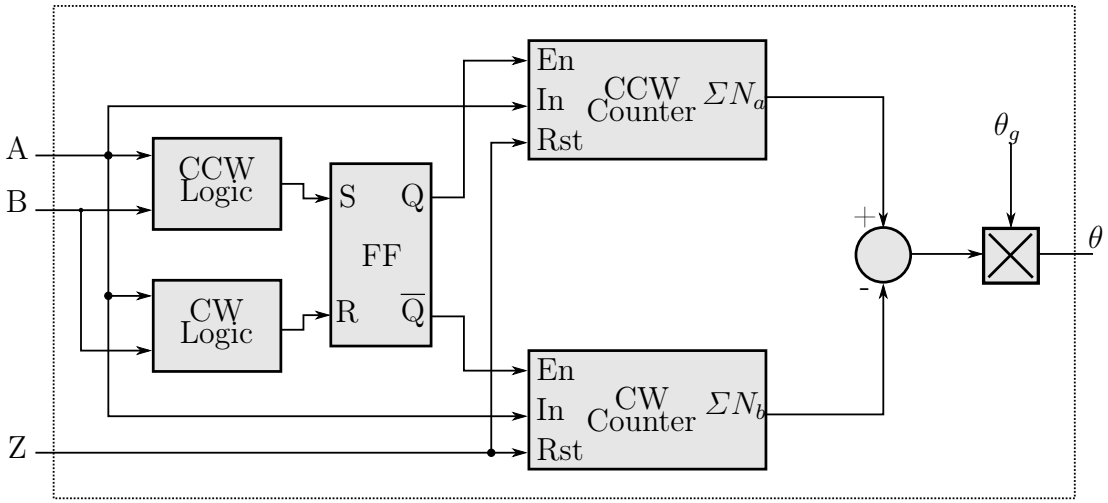

Figure 3.2: Block diagram representation of angular position calculation.

3.4 Frequency based speed decoding method

The classical and the simplest method of calculating the angular speed of a rotating shaft is by directly measuring the frequency of encoder pulses. The number of pulses are counted inside fixed time observation window. The speed is then calculated to be a discrete incremental ratio (speed is assumed to be constant inside the time observation window) as follows

$$\omega_m = \frac{\Delta\theta}{\Delta T_w} = \frac{2\pi N}{N_{pr} T_w} \tag{3.3}$$

where N is the number of counted pulses inside time observation window, and N_{pr} is the number of pulses inside one complete revolution. The T_w represents the time window during which speed is estimated based on the counted number of encoder pulses. The estimated speed is directly proportional to the encoder pulses.

The principle of the speed estimation method based on the frequency measurement technique is shown in Fig. 3.3. The main advantage of the frequency based speed decoding method is its simplicity. There is always a quantization error which is superimposed to the effective mean value of calculated speed, depending upon the uncertainty on the counted pulses. This uncertainty is because of the lack of synchronization between time observation window and the generated encoder pulses. The quantization error in the speed is the ratio of measured speed ω_m and counted number of pulses N. Mathematically, it is derived as

$$\Delta Q_\omega = \frac{\omega_m}{N} = \frac{2\pi}{N_{pr} T_w} \tag{3.4}$$

It can be noticed from (3.4), that the quantization error does not depend on the speed. It depends only on the number of encoder pulses per revolution and the speed

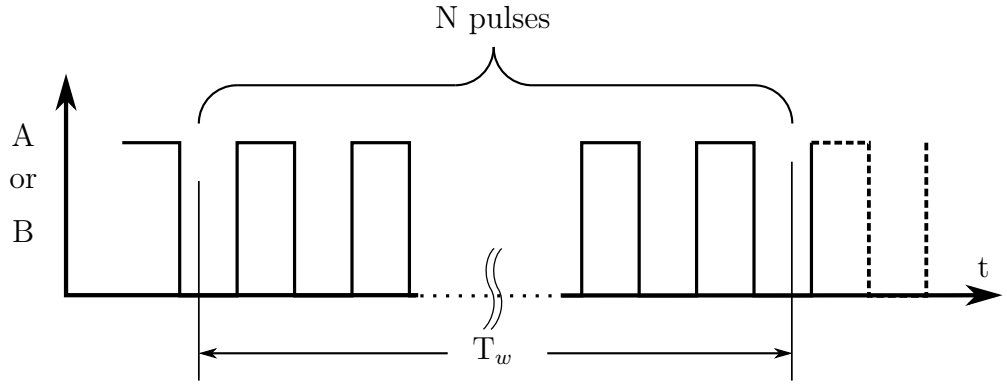

Figure 3.3: Speed estimation principle based on frequency measurement method.

sampling time (time window T_w). However, for this method of speed calculation, the relative error is the ratio of the quantization error and measured speed itself [3]:

$$\varepsilon_{fm} = \frac{\Delta Q_\omega}{\omega_m} = \frac{2\pi}{\omega_m N_{pr} T_w} \tag{3.5}$$

The Equation (3.5) clearly shows that the relative error increases as the rotational speed decreases. At high speeds, the error almost negligible. This is because, at high speeds, the counted number of pulses inside the time measurement window is high. Thus, the frequency measurement method is most suitable for high speed applications only.

A block diagram representation for speed and error computation based on the frequency measurement method is shown in Fig. 3.4. A fixed time window (speed sample time) pulse is generated based on which, two up counters are reset and enabled in order to count the number of pulses. The counted pulse number from the

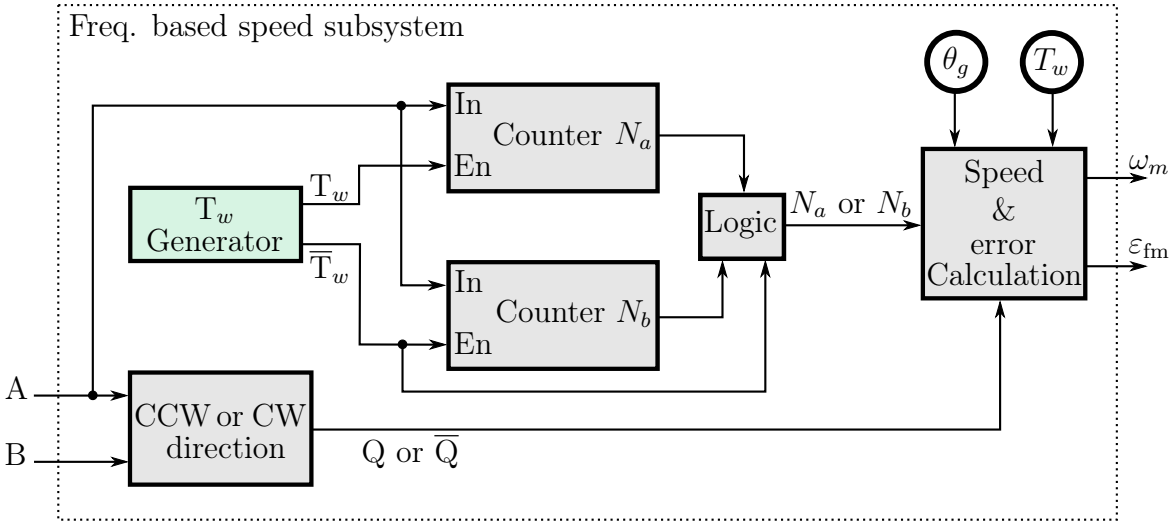

Figure 3.4: Block diagram representation for speed calculation based on the frequency measurement method [7].

just disabled counter is then processed according to (3.4) and (3.5) to calculate the speed and relative error. The value of the speed is either positive (CCW, if Q=1) or negative (CW, if $\overline{\text{Q}}$=1) depending upon the direction of the rotation signal. The implementation of this method to extract speed information is very simple, and requires only the calculation of N, which is further multiplied with constant terms in (3.3). Another similar approach is to use the block diagram representation for angular position calculation. Once angular position is calculated, speed is computed using (3.3).

3.5 Period measurement based speed decoding method

As discussed in Section 3.4, the frequency measurement technique is not suitable in a lower speed region because of the quantization error. The relative error is highest in the low to very low speed region. An alternative approach to overcome this problem, is to use the period measurement method.

In the period measurement method, a high frequency clock pulse is generated in parallel to the encoder pulse signal. The number of periods of the high frequency signal are then calculated in one (or more) encoder pulse [2,3,7]. This main principle of the period measurement method is shown in Fig. 3.5.

Considering the constant speed and a single period length of encoder signal, the angular speed can be estimated as

$$\omega_m = \frac{\Delta\theta}{\Delta t} = \frac{\Delta\theta}{nT_h} = \frac{2\pi}{N_{pr} n T_h} \tag{3.6}$$

where T_h is the time period of the high frequency pulse and n represents the number of periods of the high frequency signal. Therefore, a sample of the speed can be taken at each period of the encoder pulse. In this way, the speed sample time becomes

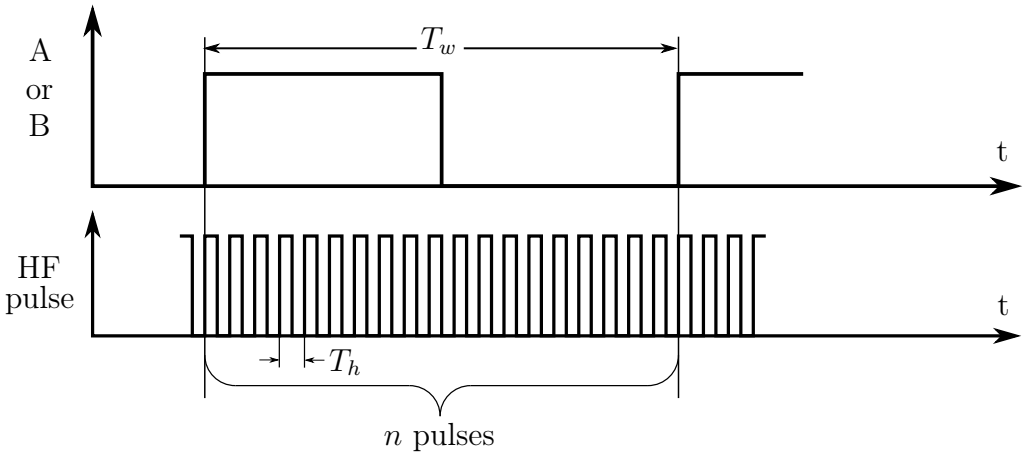

Figure 3.5: Speed estimation principle based on the period measurement method [7].

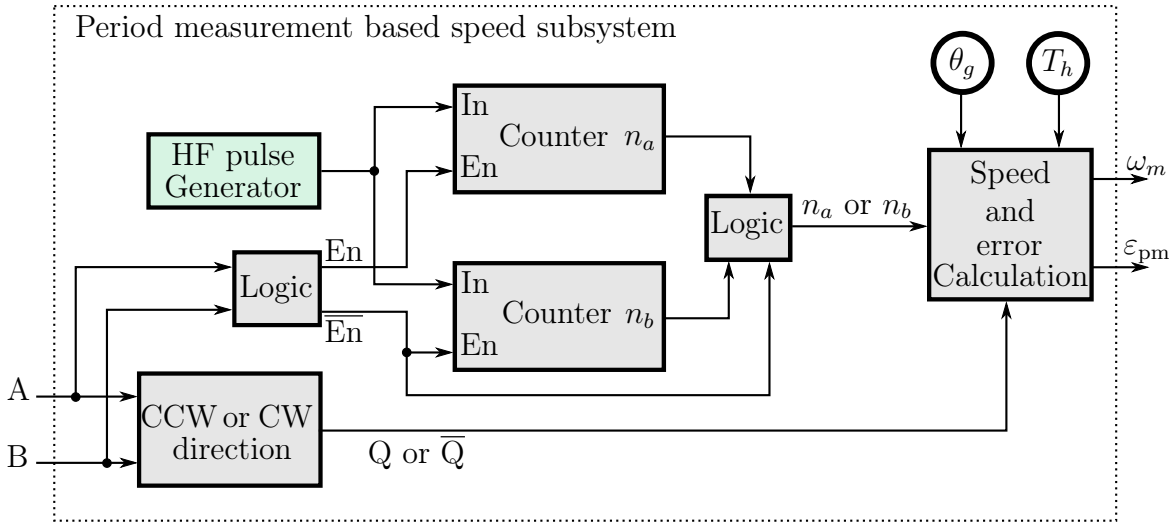

Figure 3.6: Block diagram representation for the speed calculation based on the period measurement method [7]

the function of angular speed. Mathematically it is expressed as [3]

$$T_w(\omega_m) = \frac{2\pi}{N_{pr}\omega_m} \tag{3.7}$$

As the speed increases, the encoder pulse width decreases, hence speed sample time also decreases. The measurement accuracy of the speed is depending on the ratio of the high frequency counter period and that of the signal generated by the encoder [3]. The percentage and absolute errors are difficult to calculate due to the involvement of non-linear rounding functions. The relative error is proportional to the angular frequency of motor and is given as [3]

$$\varepsilon_{pm} = \frac{\omega_m N_{pr} T_h}{2\pi} \tag{3.8}$$

where ε_{pm} represents the relative error for the period measurement method. Equation (3.8) cleary shows that in low speed region, error is negligibly small, while it increases with the increase of a rotational speed.

A block diagram representation for the period measurement method is presented in Fig. 3.6. It is similar to that of the frequency measurement method (Fig. 3.4). The only difference is that, the high frequency clock pulses are counted instead of encoder pulses, in one or more encoder pulse width duration. The speed is then computed from (3.6) by multiplying the counts with constant terms. This method is most suitable for the low speed region and introduces error at high speeds.

3.6 Combined method for speed computation

Both the frequency and period measurement methods are applicable to limited speed ranges. For example, accuracy of the frequency measurement technique is higher

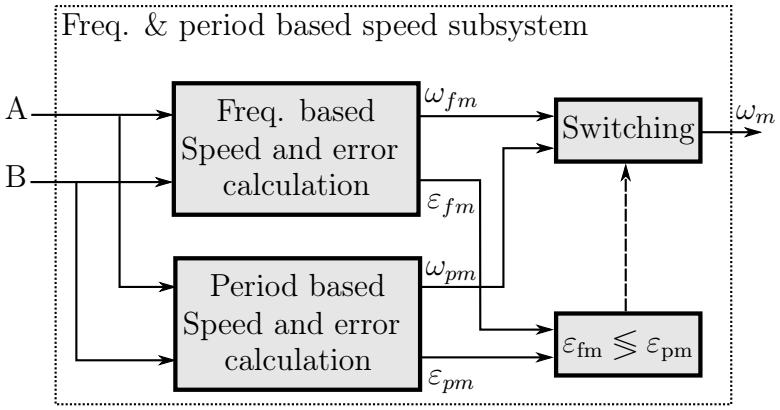

Figure 3.7: Block diagram representation based on the combined (frequency and period measurement) method for speed measurement.

at high speeds, and vice versa for the period measurement method. It is therefore required to develop an algorithm which would be applicable to all speed ranges with negligible relative error. A trivial solution is to use high frequency period measurement method in the low speed region which switches to the frequency measurement method as the speed increases. The switching action is introduced at a point where the relative error for both methods becomes equal to each other ($\varepsilon_{pm} = \varepsilon_{fm}$). Thus, by making the (3.5) and (3.9) equal to one another, the critical speed value can be solved as

$$\omega_{crit} = \frac{2\pi}{N_{pr}} \cdot \frac{1}{\sqrt{T_w T_h}} \tag{3.9}$$

A block diagram representation for the combined method is shown in Fig. 3.7. It is shown that both the frequency and period measurement methods are used to compute speed and relative error. While a switching operation to select the best speed computation subsystem is modeled by comparing the relative errors of both methods.

This method combines the advantages of the methods presented in Section (3.4) and (3.5). Not only encoder pulses are measured, but also the high frequency clock pulses in a fixed time duration. The compensation of the relative errors introduced by the sampling time may increase the accuracy in the final measurement. This technique to calculate speed is very straightforward and implementation is easy. However, at very low speed, it affects the system performance by intermittent speed feedback. A sophisticated switching mechanism which changes the position from one method to other in a very short time interval is necessary to get the continuous speed samples. Moreover, the quantization error is still present when using frequency measurement method.

3.7 Pulse-window synchronisation method

A speed decoding algorithm is presented in [3, 12, 23] which introduces very low relative error in comparison to previously mentioned algorithms. The main advantage of this method is that the same algorithm can be used for wide speed ranges without requiring switching mechanism. It uses the frequency measurement method while compensating for quantization error. The quantization error exists because the speed calculation time window and the encoder pulses are not synchronised. In order to completely remove the quantization error, the time period between bounds of the time window and the incremental encoder generated pulse is measured. Based on this, a new time window can be adopted for speed calculation, which leads to integer number of pulse counts, thus zeroing the quantization error.

The concept is presented in Fig. 3.8. The encoder pulses are counted in a fixed time interval (time observation window) given as T_w. The time difference between bounds of the basic time window and the encoder pulses is then measured as ΔT_{h-1} and ΔT_h. Based on these time differences, a new time window is then adopted for speed computation. While, in order to obtain high accuracy, the basic time window (T_w) is assumed in such a way, that at least one pulse is detected within this duration. In case, no pulse falls in this window (low speed region), the basic time window is then extended to its integer multiple until at least one pulse is received. The newly adaptive time window (T_{eq}) will be based on this extended basic window. For example, considering sampling instant $h-1$, the new adaptive observation window is given as

$$T_{eq,k-1} = \Sigma T_w + (\Delta T_{h-1} - \Delta T_h) \tag{3.10}$$

The extention of width of basic time observation window (T_w) is prestented as ΣT_w. The speed is then estimated by the formula given as

$$\omega_m = \frac{N}{\Sigma T_w + (\Delta T_{h-1} - \Delta T_h)} \frac{2\pi}{N_{pr}} \tag{3.11}$$

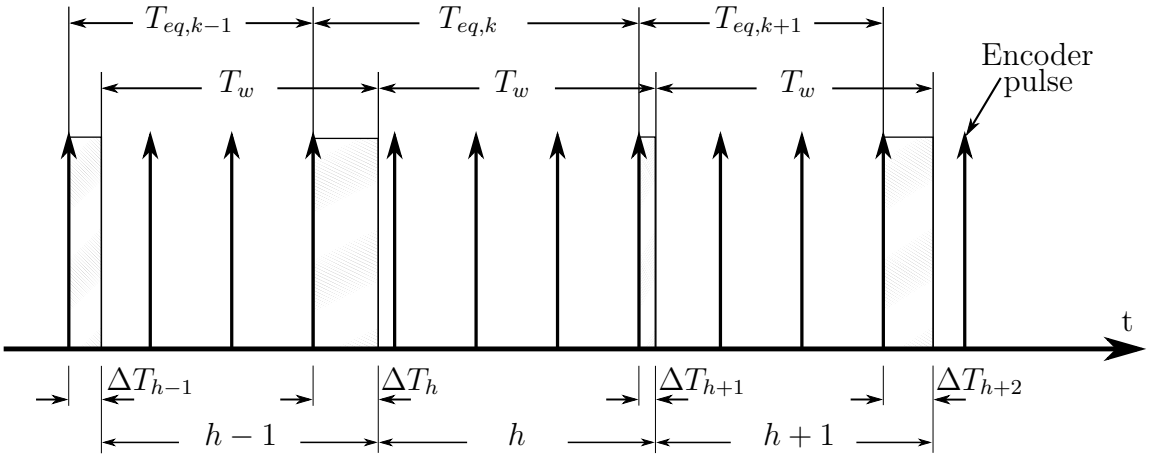

Figure 3.8: Principle of pulse-window synchronisation method.

In this algorithm, the same kind of time duration is calculated inside each cycle. A block diagram representation is shown in Fig. 3.9. A fixed time observation window is generated in the form of a pulse. With the start of the encoder signal, the counter starts counting the pulses. A specific logic is implemented to find at least one encoder pulse inside the time window. This is done by checking the encoder output at every rising edge of T_w. The counter is then reset only when the encoder output is non zero, as the rising edge is arrived. Otherwise it keeps counting. The reset pulse is generated by comparing the counter output and T_w. It is always integer multiple (ΣT_w) of the generated time window (T_w).

The bounds between the incoming encoder pulses and fixed or extended time window (ΔT_{h-1} and ΔT_h) is then calculated. Based on the extended time window and the time duration between bounds, a new window is adopted according to (3.10) which is further used for speed calculation in (3.11). To detect the rotation direction reversal, a separate subsystem is needed as used in previous methods which provides information for the final speed computation block. In this technique, the quantization error is introduced only during time period calculation.

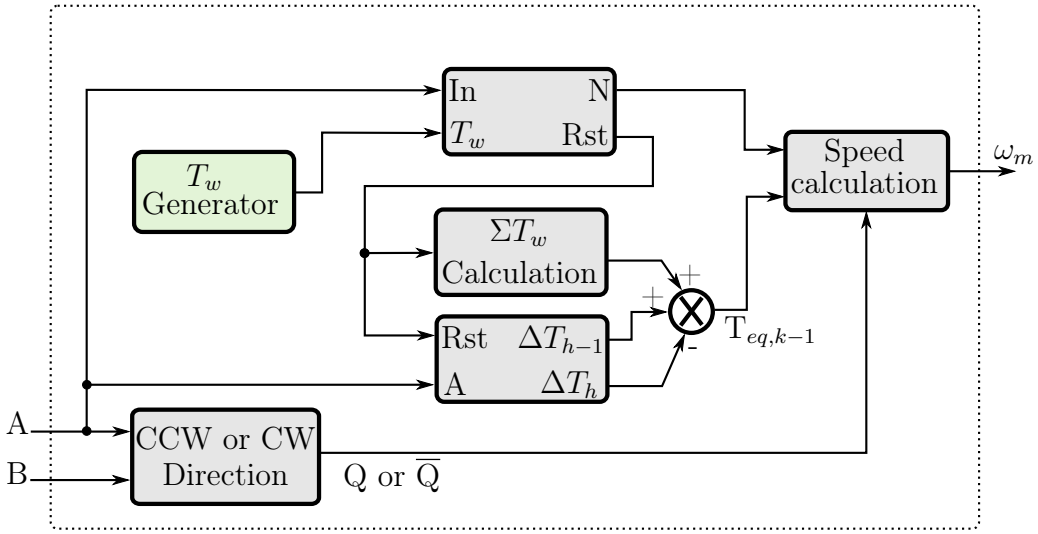

Figure 3.9: Block diagram representation for pulse-window synchronization method.

4 Simulink implementation

The speed decoding algorithms presented in the previous section are implemented in Matlab Simulink environment and the obtained results are described in this section. The behavior of all these algorithms is further investigated under different case scenarios. Finally, a comparative analysis is done based on accuracy and functional limitations of each. For all these simulation, an incremental shaft encoder block from Simulink library is used. Its resolution can be adjusted. The input reference speed signal is a sinusoidal signal with frequency of 8.976 rad/s. A sinusoidal input is chosen for all simulations in order to analyze the results in clockwise and anticlockwise directions.

4.1 Frequency measurement method

Frequency measurement method is implemented in Matlab Simulink. The resolution of the incremental shaft encoder is set at 2048 ppr which is typical value for general purpose optical incremental encoders. The input speed signal maximum amplitude is set at 3000 rpm and the speed sample time window is fixed as $T_w = 1$ms.

The resulted calculated speed response based on frequency measurement method is shown in Fig. 4.1 (upper figure). With above mentioned parameters, the frequency measurement method holds good in normal speed operation, since the calculated speed perfectly follows the reference speed signal. The rotation direction reversal behavior is also being detected by the algorithm. The relative error is also shown in Fig. 4.1 (lower figure). It can be noticed that the relative error from (3.5) is high in the low speed region and decreases with an increase in the angular speed.

Further investigation especially in the high speed region, is required in comparison with low speed range. In order to analyze the implmeneted algorithm in high speed region, the amplitude of the input signal is set at 10000 rpm, while the resolution of incremental encoder is also increased to 4000 rpm. The resulted speed response is shown in Fig. 4.2. The time observation window is set at 1 ms. The resulted speed plot is more smooth compared with the previous one in Fig. 4.1. The

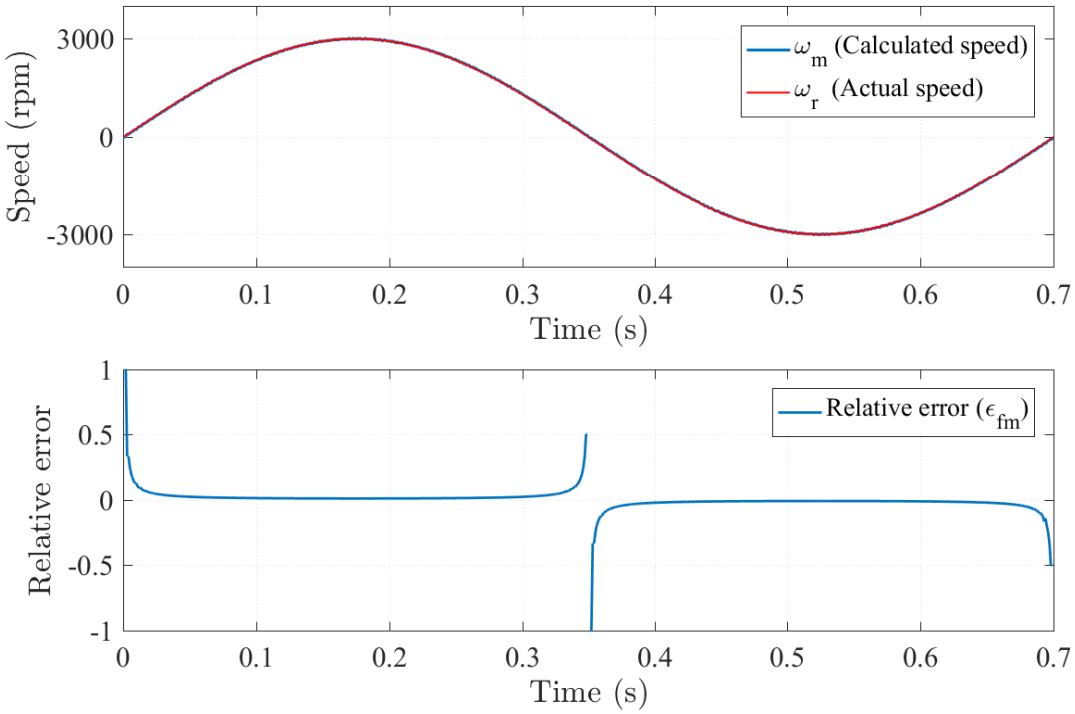

Figure 4.1: Frequency measurement method: speed response (upper figure) and relative error plot (lower figure) for $T_w = 1$ ms, $N_{pr} = 2048$ ppr.

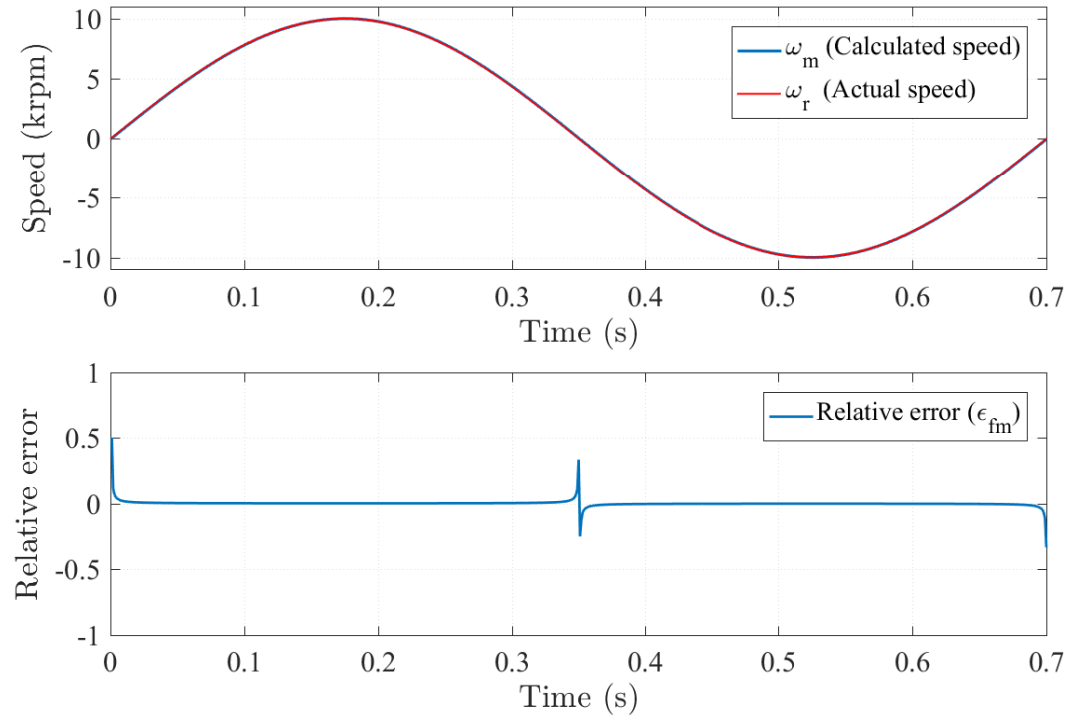

Figure 4.2: Frequency measurement method: speed response (upper figure) and relative error plot (lower figure) for $T_w = 1$ ms, $N_{pr} = 4000$ ppr

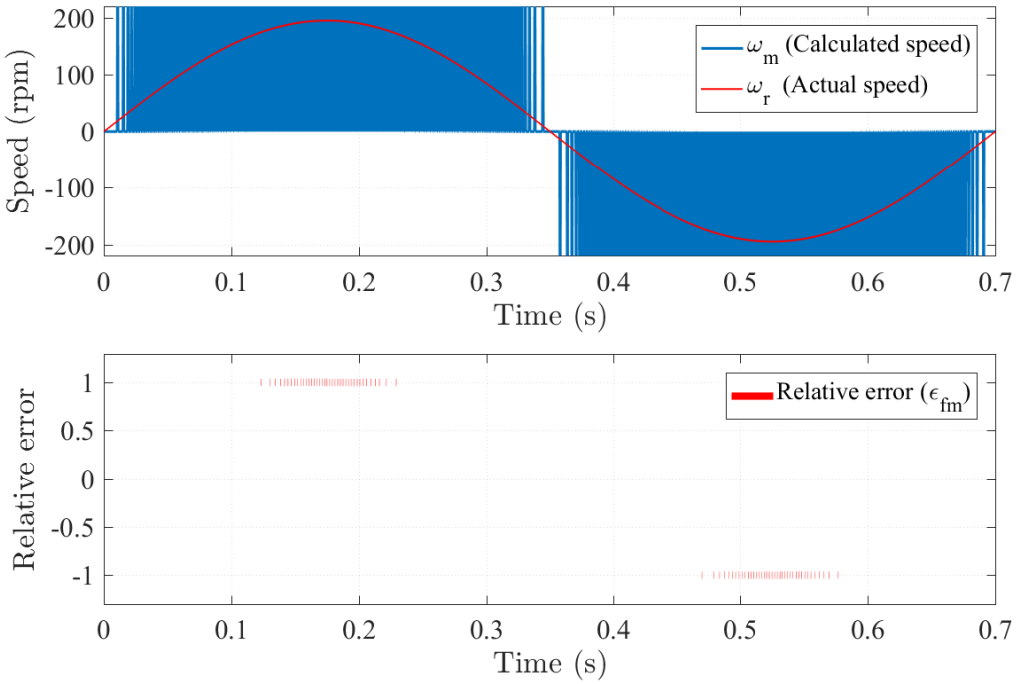

Figure 4.3: Frequency measurement method: speed response (upper figure) and relative error plot (lower figure) for $T_w = 0.3$ ms, $N_{pr} = 590$ ppr.

relative error further decreases as the speed approaches to its peak. To investigate the response of frequency measurement method in low speed region, input speed signal amplitude is adjusted at $\omega_r = 195$ rpm and a low resolution incremental encoder is used (e.g $N_{pr} = 590$ ppr). This is the most difiicult operational region for frequency measurement method. The resulted speed response is shown in Fig. 4.3. It can be noticed from Figs. 4.2 and 4.3 that the frequency measurement based speed decoding method can be most suitable choice for high speed regions only. It gives high relative error at low speed with low resolution incremental encoders.

4.2 Period measurement method

As discussed in Section 3.5, the period measurement method performs well in the low speed region unlike the frequency measuremend based method for the speed caluclation. The period measurement algorithm for the speed calculation is implemented in Simulink according to the block diagram representation in Fig. 3.6. The resulted speed response to a sinusoidal input signal is shown in Fig. 4.4. The time period of high frequency pulse signal T_h is set at 1μs. The resolution of the encoder is 2048 ppr and the amplitude of the input speed signal is 3000 rpm. This simulation is performed to check the overall behavior of the period measurement method in increasing, decreasing, clockwise and anticlockwise regions. It can be noticed that the calculated speed response is smooth and follows the reference speed signal well up to a specific speed range. After that, it loses its quality with further increase in

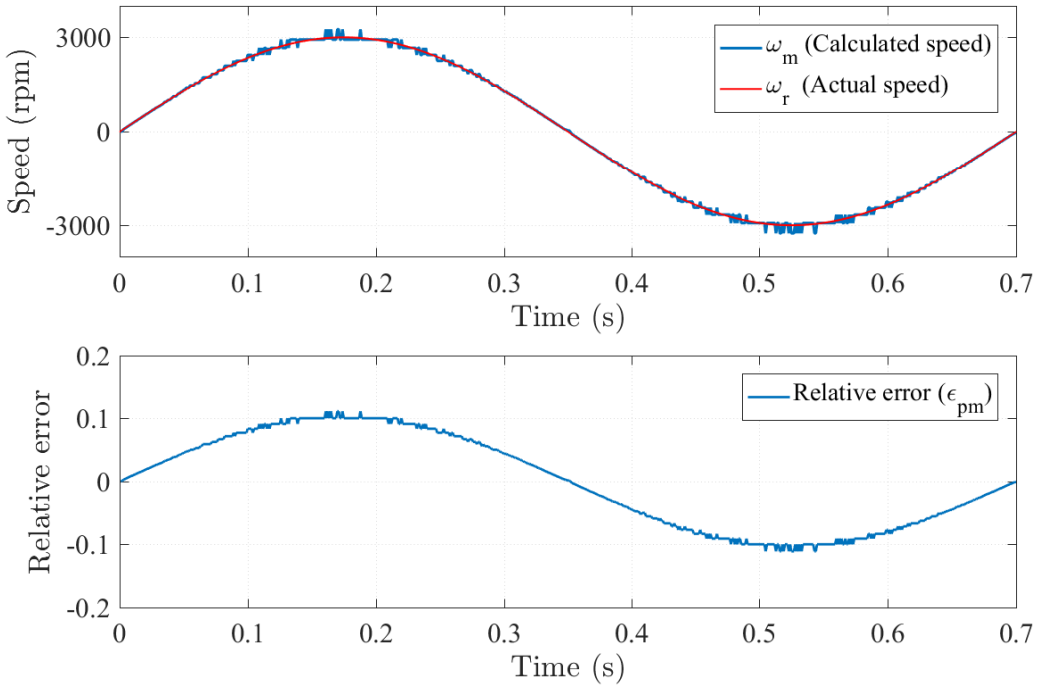

Figure 4.4: Period measurement method: speed response (upper figure) and relative error plot (lower figure) for $T_h = 1$ μs, $N_{pr} = 2048$ ppr.

the speed.

The relative error is also shown in Fig. 4.4 (lower figure). It increases with an increase in speed. It is because of quantization error which increases as the number of periods of high frequency clock pulses decrease in one encoder pulse time period [2]. To analyze the response of period measurement method based speed decoding algorithm in high speed range, an input sinusoidal speed signal with maximum amplitude of 10000 rpm is applied to the incremental encoder. The incremental encoder resolution is set to 4000 ppr to examine the behavior of the algorithm with minimum encoder pulse width. The time period of high frequency clock signal is set in such a way that at maximum speed, the T_h should be less than the time period of one encoder pulse. At 10000 rpm speed with encoder resolution of 4000 ppr, the shorter encoder pulse width will be 1.5 μs. It is calculated as [7]

$$T_e = \frac{2\pi}{\omega_{\rm r} N_r} \tag{4.1}$$

The encoder pulse width reduces with an increase in rotational speed. Accordingly, the T_h is set at 0.1 μs. The resulted response is shown in Fig. 4.5. It can be noticed that the accuracy of this algorithm suffers at high speed.

Fig. 4.6 shows the speed response in low speed range for $T_h = 1$ μs, $N_{pr} = 590$ ppr and $\omega_{\rm r} = 195$ rpm. In comparison with the frequency measurement algorithm for the same parameters (c.f. Fig. 4.3), the period measurement method provides a much better result. The relative error is negligibly small in the period measurement method in the low speed range.

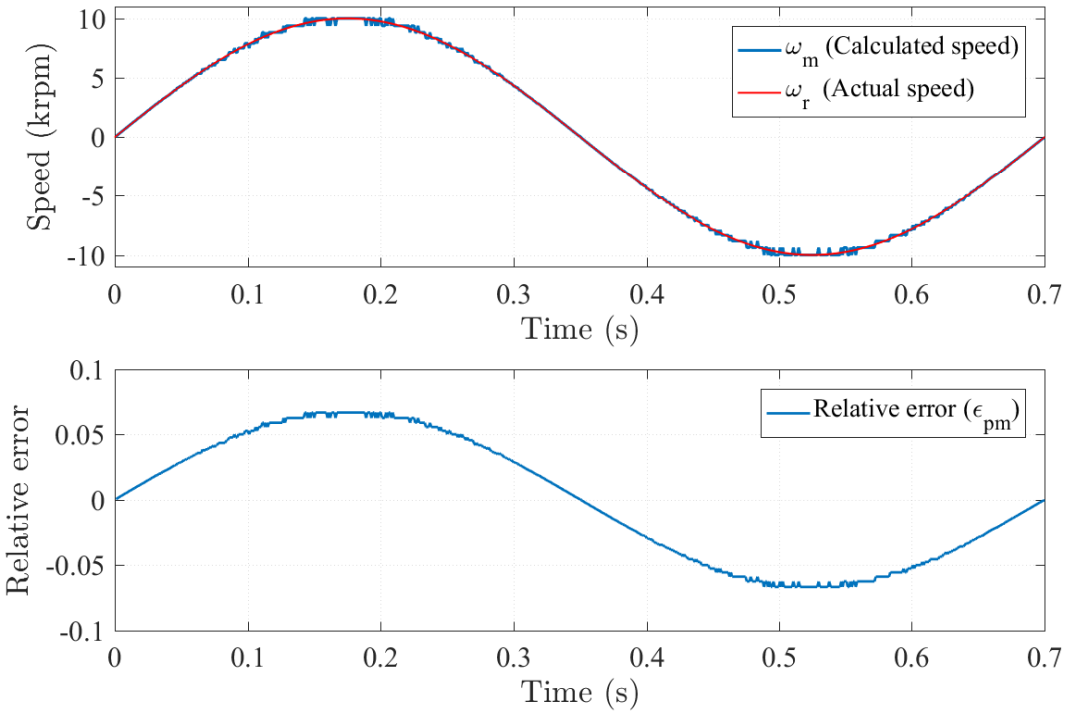

Figure 4.5: Period measurement method: speed response (upper figure) and relative error plot (lower figure) for T_h=0.1 μs, N_{pr}=4000 ppr.

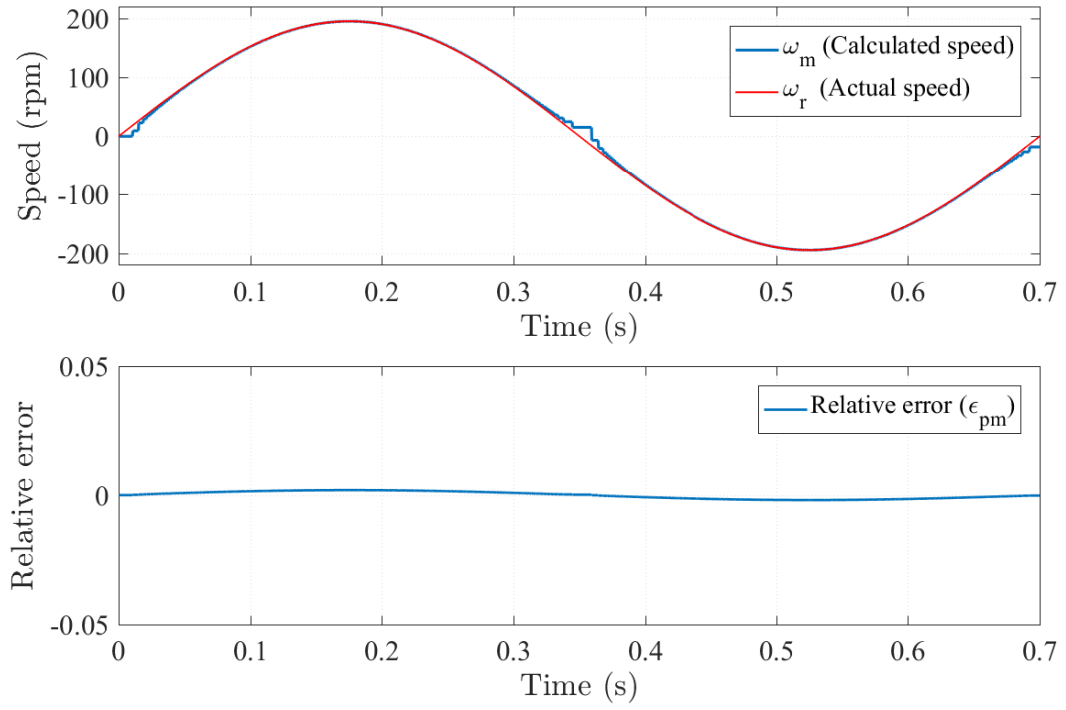

Figure 4.6: Period measurement method: speed response (upper figure) and relative error plot (lower figure) for $T_h = 1$ μs, $N_{pr} = 590$ ppr.

4.3 Combined method

The mixed mode speed decoding method combines the advantages of both the frequency and period measurement methods. The accuracy of the speed response is thus increased in all speed regions. The speed response based on combined method for $T_w = 1$ ms, $T_h = 1$ μs, $N_{pr} = 2048$ ppr and $\omega_r = 3000$ rpm is shown in Fig. 4.7. The algorithm uses the time period measurement method in low speed range and switches to frequency measurement method as the speed increases. The switching action is determined by comparing the relative error for both methods. A cross-over point is reached where relative error for period measurement method (ε_{pm}) becomes equal to that of frequency measurement method (ε_{fm}).

After that point, if the speed is further increased, the ε_{fm} becomes smaller than ε_{pm} and the algorithm starts using the frequency measurement method for the speed computation. Therefore, the accuracy of the resulted speed response increases in both regions. The relative error for both methods are opposite to each other.

Fig. 4.8 presents the speed plots for the frequency and time period based measurement based methods along with the relative error plot. It clearly shows that the accuracy for period measurement method reduces at higher speeds and switching happens to frequency measurement method when $\varepsilon_{pm} > \varepsilon_{fm}$.

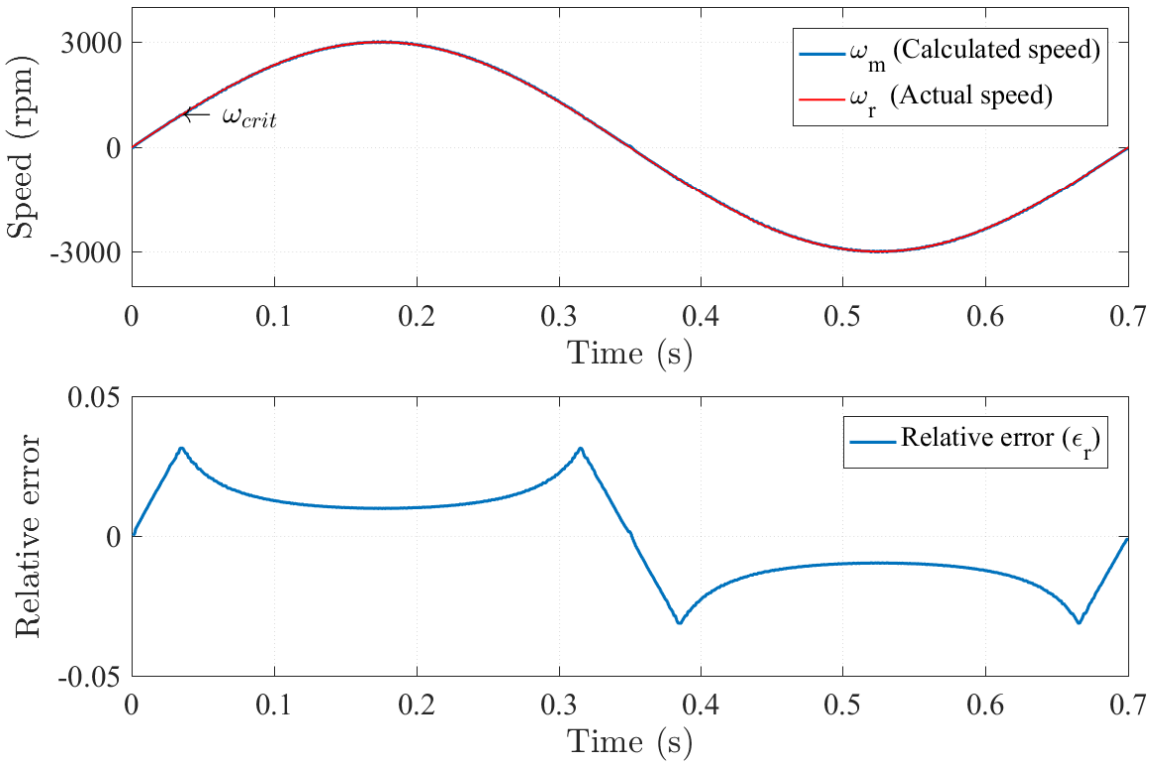

Figure 4.7: Combined method: speed response (upper figure) and relative error plot (lower figure) for $T_w = 1$ ms, $T_h = 1$ μs, $N_{pr} = 2048$ ppr.

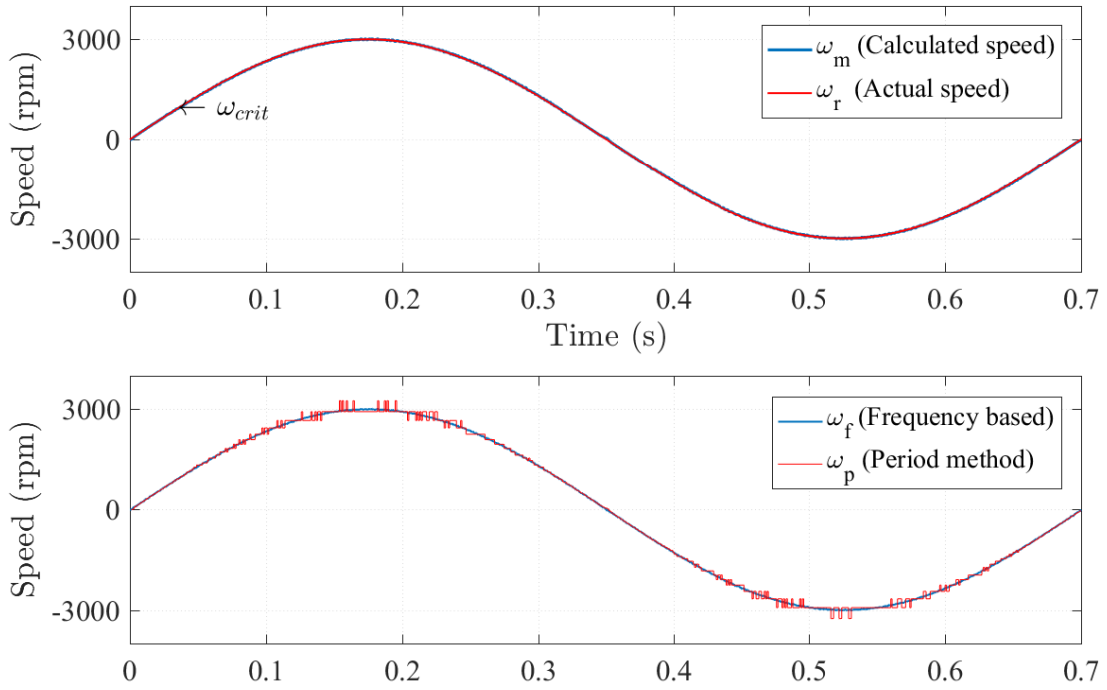

Figure 4.8: Combined method with frequency and period measurement method speed responses: for $T_w = 1$ ms, $T_h = 1$ μs, $N_{pr} = 2048$ ppr.

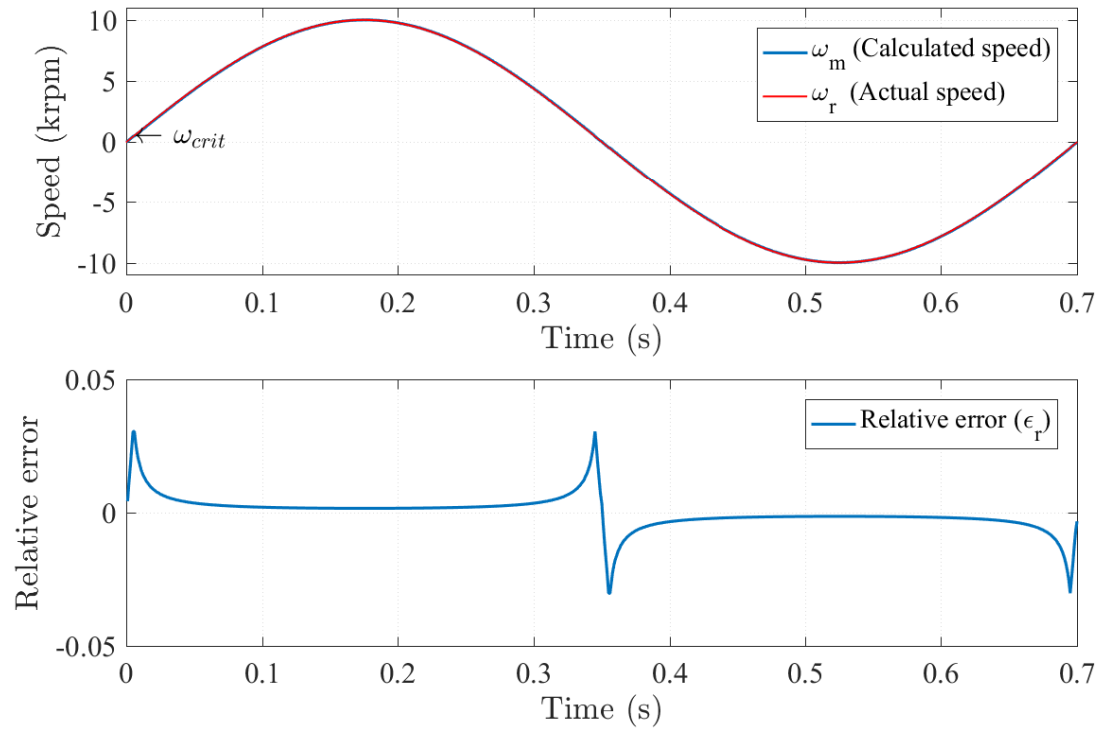

Figure 4.9: Speed response (upper figure) and relative error plot (lower figure) for $T_w = 1$ ms, $T_h = 0.1$ μs, $N_{pr} = 4000$ ppr.

The behavior of the combined method based speed decoding is examined in high speed range. The resolution of the incremental encoder is 4000 ppr and an input sinusoidal speed signal of amplitude 10000 rpm is applied. The resulted speed response to $T_w = 1$ ms, and $T_h = 0.1$ μs is shown in Fig. 4.9. The resulted speed response and relative error plot is no more different than in Fig. 4.7. The results show that the combined method performs well in high speed range. Fig. 4.10 presents the speed plot for both frequency and period measurement methods along with their relative error plots. It can be noticed that the relative error for frequency measurement method approaches zero at maximum speed. On the other hand, the period measurement method accuracy suffers at high speeds.

Further to explore the behaviour of combined method for speed computation in low speed range, a simulation test is performed for $T_w = 0.3$ ms, and $T_h = 1$ μs, $N_{pr} = 590$ ppr and $\omega_{\mathrm{r}}(\mathrm{max}) = 195$ rpm. The resulted speed response is shown in Fig. 4.11. The result shows that at very low speeds, the time period measurement method with low resolution incremental encoder holds good but the speed value is updated only when the new encoder pulse signal starts. The relative error is very small for period measurement method compared with that of the frequency measurement method. The relative error for the frequency measurement method is visible only when the speed approaches to its maximum value of 195 rpm and is very

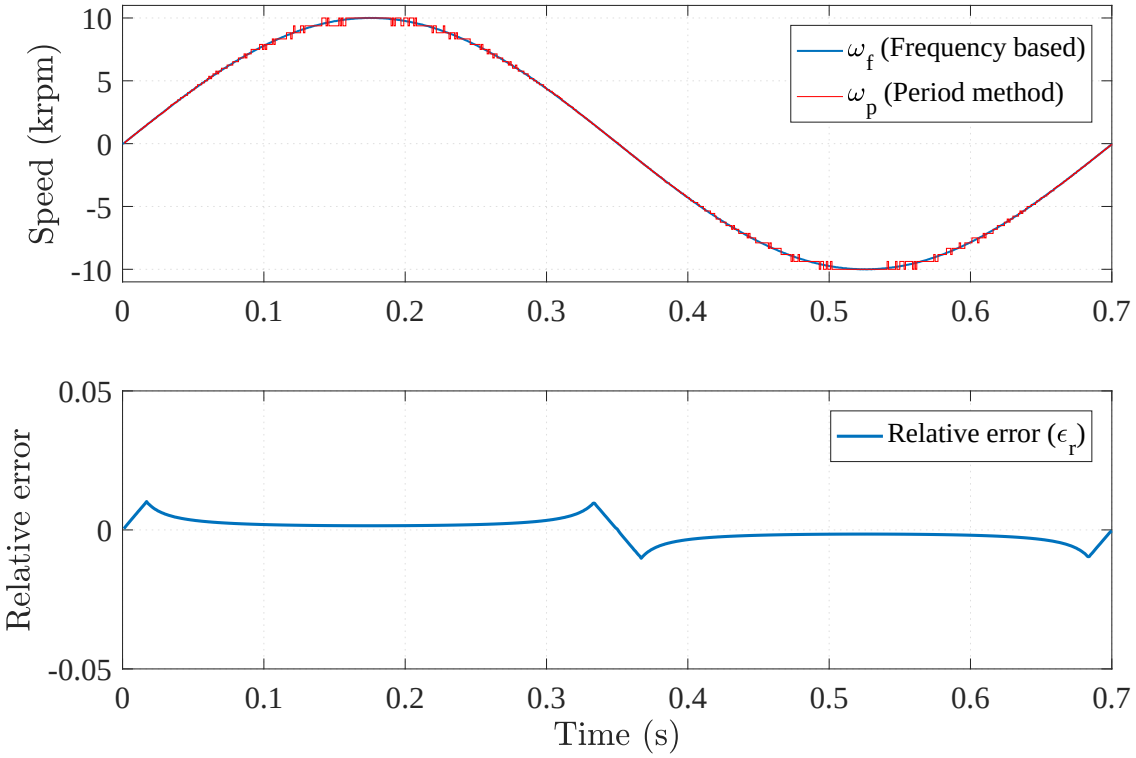

Figure 4.10: Frequency and period measurement method based speed response (upper figure) and relative error plot (lower figure) for $T_w = 1$ ms, $T_h = 0.1$ μs, $N_{pr} = 4000$ ppr.

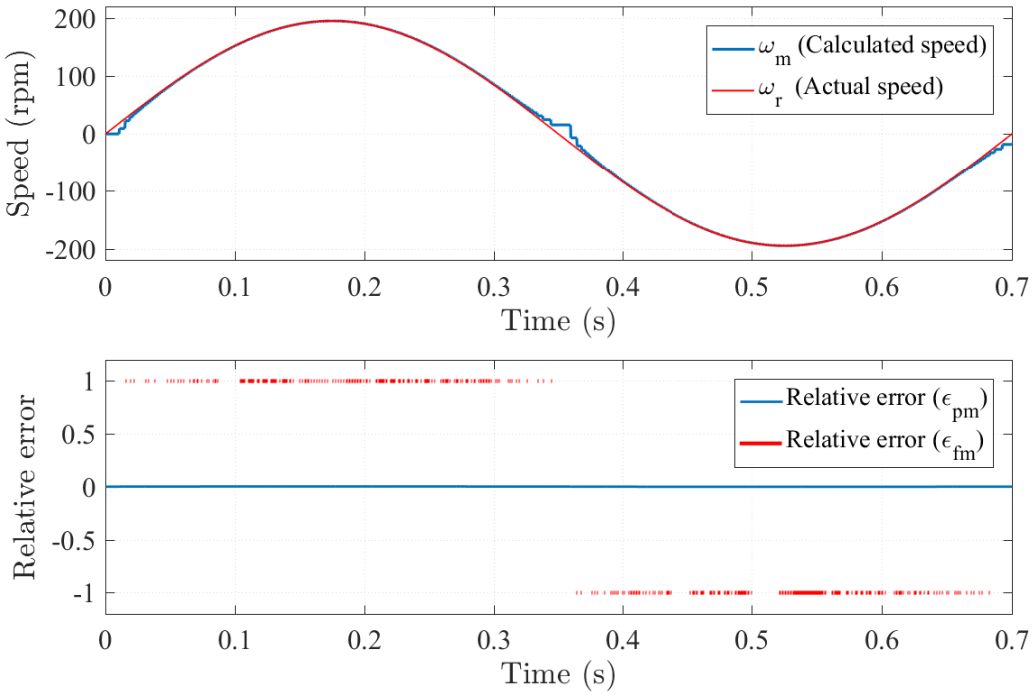

Figure 4.11: Speed response (upper figure) and relative error plot (lower figure) for $T_w = 0.3$ ms, $T_h = 1$ μs, $N_{pr} = 590$ ppr.

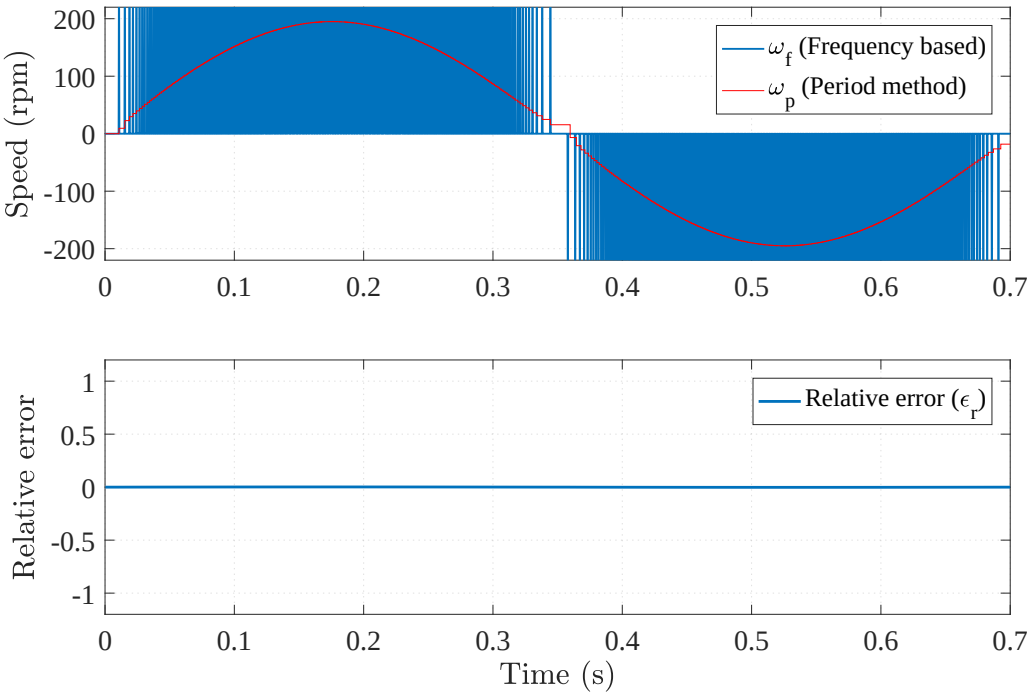

Figure 4.12: Frequency and period measurement method based speed response (upper figure) and relative error plot (lower figure) for $T_w = 1$ ms, $T_h = 1$ μs, $N_{pr} = 590$ ppr.

high at very low speeds. In this case, there is no cross-over point, and therefore the combined method uses the period measurement method only.

On the other hand, the frequency and the speed measurement based speed responses along with their relative errors is shown in Fig. 4.12. It can be noticed that the period measurement method is way better than the frequency measurement method at very low speeds.

4.4 Pulse-window synchronization method

As discussed in Section 3.7, the pulse-window synchronization uses the frequency measurement method while compensating for the quantization error problem at the same time. A sinusoidal input signal is applied with maximum amplitude of 3000 rpm. The incremental encoder resolution is set at 2048 ppr. For $T_w = 1$ ms, the speed response of pulse-window synchronization algorithm is shown in Fig. 4.13. The high frequency clock period T_h required for period measurements is set at 0.1 μs.

The speed response is quite promising and quantization error due to lack of synchronization between encoder pulse and the time window is removed in comparison with classical frequency measurement method. However, the only quantization error is introduced during time period measurement by the counters. These counters are used to measure the time periods required to calculate the newly adaptive

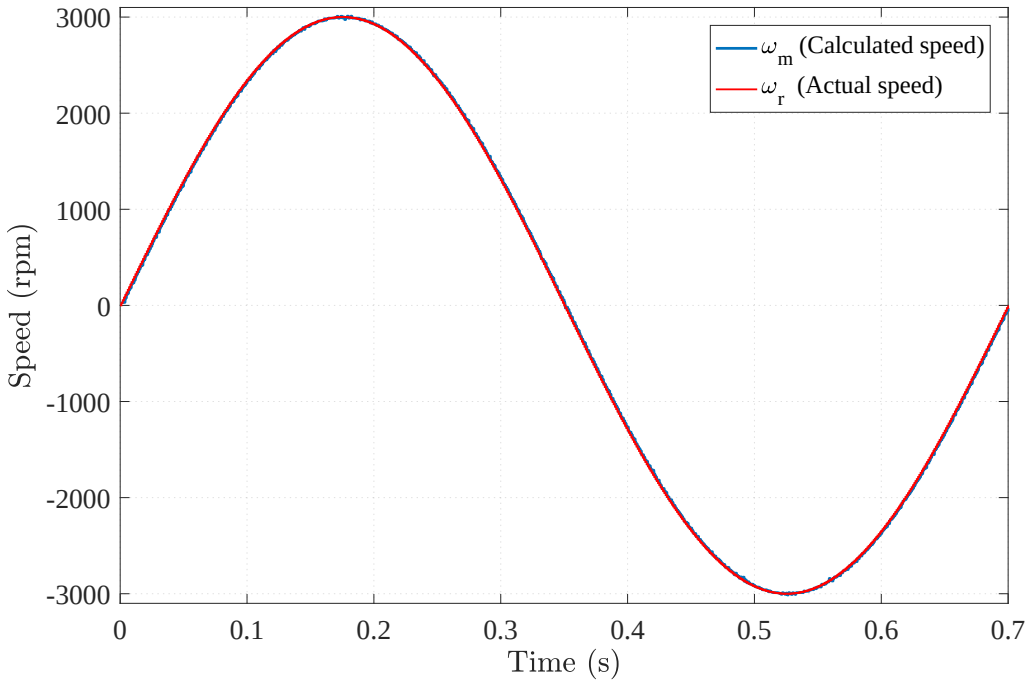

Figure 4.13: Pulse-window synchronization method: speed response for $T_w = 1$ ms, $T_h = 0.1$ μs, $N_{pr} = 2048$ ppr.

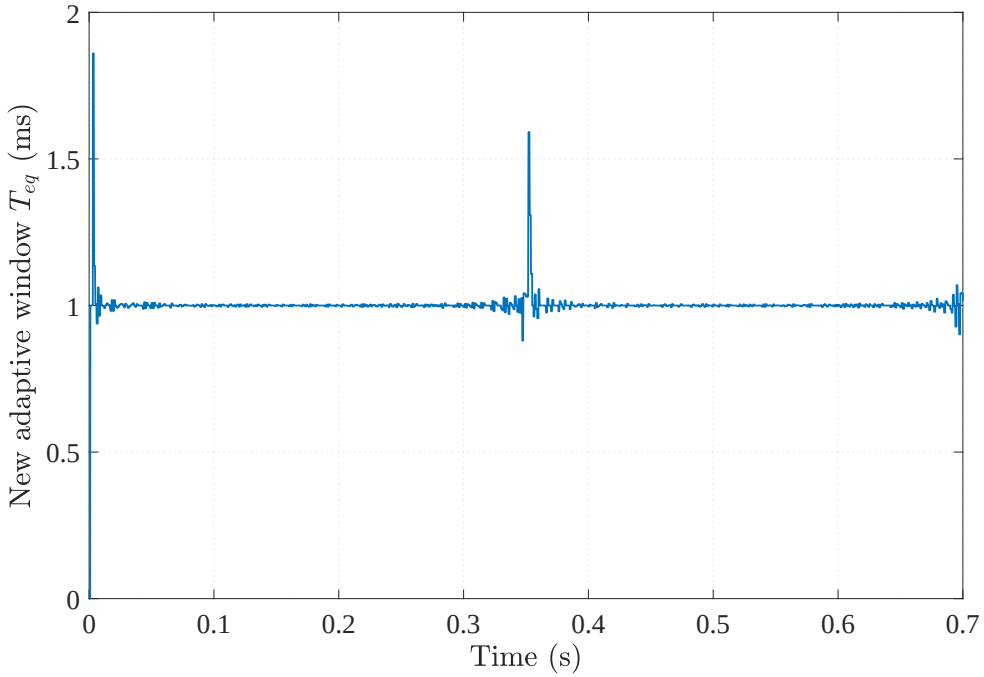

Figure 4.14: Pulse-window synchronization method: new observation window plot for $T_w = 1$ ms, $T_h = 0.1$ μs, $N_{pr} = 2048$ ppr.

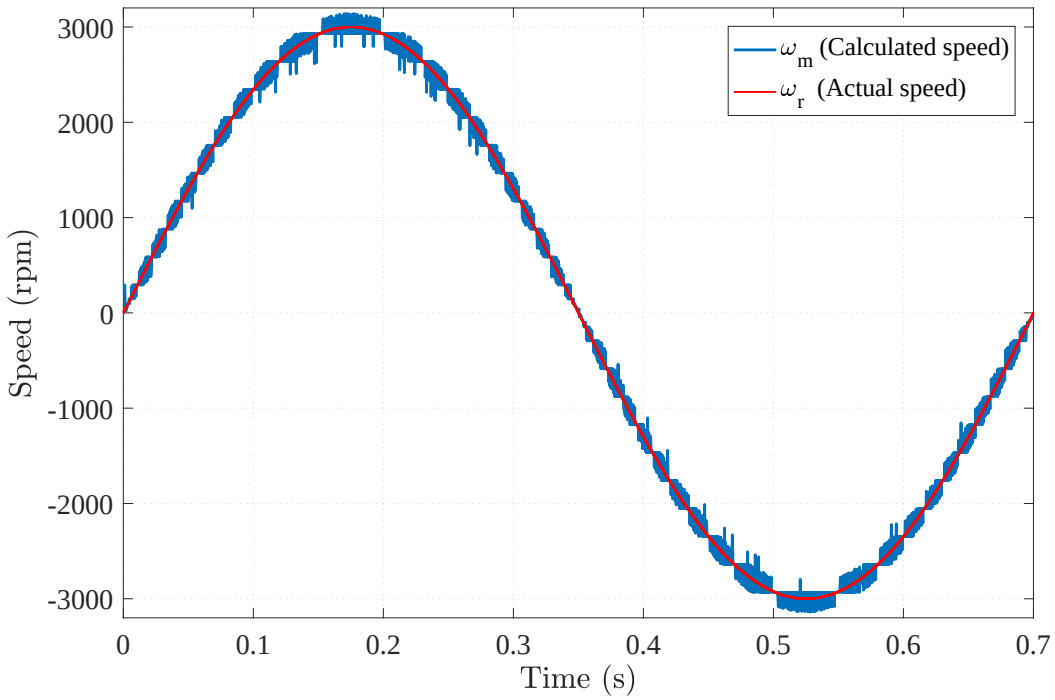

Figure 4.15: Pulse-window synchronization method: speed response for $T_w = 0.1$ ms, $T_h = 0.1$ μs, $N_{pr} = 2048$ ppr.

window. The newly adaptive time window in corresponding to Fig. 4.13 is plotted in Fig. 4.14. In can be noticed that in the start at low speeds that time window increases in order to get atleast one pulse and then settles to its basic width (T_w). In comparison with encoder pulse width, the basic time window should be adjusted so that maximum number of the encoder pulses should fall in it. In order to examine the effect of time window width on the speed response by pulse-window synchronization method, the basic time window is now reduced to 0.1 ms. The resulted response is shown in Fig. 4.15. It can be noticed that with the reduced basic time window, the calculated speed response starts fluctuating. It is because less number of encoder pulses are counted in each basic time window, while at the new time window changes itself according to (3.10). The correct sampling of data required for the speed calculation is a challenging task in this method.

In Fig. 4.16, the newly adaptive time window T_{eq} is presented for $T_w = 0.1$ ms, $T_h = 0.1$ μs, $N_{pr} = 2048$ ppr and $\omega_{\mathrm{r}}(\mathrm{max}) = 3000$ rpm. It shows that in the start at low speeds, the basic time window is extended from 0.1 ms to 1.4 ms in order to get at least one encoder pulse. As the speed increases, the frequency of the encoder pulse signal also increases and the basic time window is sufficient to gather one encoder pulse. The new time window is therefore the sum of the single basic time window and the time bounds between encoder pulse and the basic time window at high speeds (for example from $t = 0.1$ to 0.3 s).

Fig. 4.17 shows the speed response by pulse-window synchronization method for $T_w = 1.5$ ms, $T_h = 0.1$ μs, $N_{pr} = 4000$ ppr and $\omega_{\mathrm{r}} = 10000$ rpm. The result

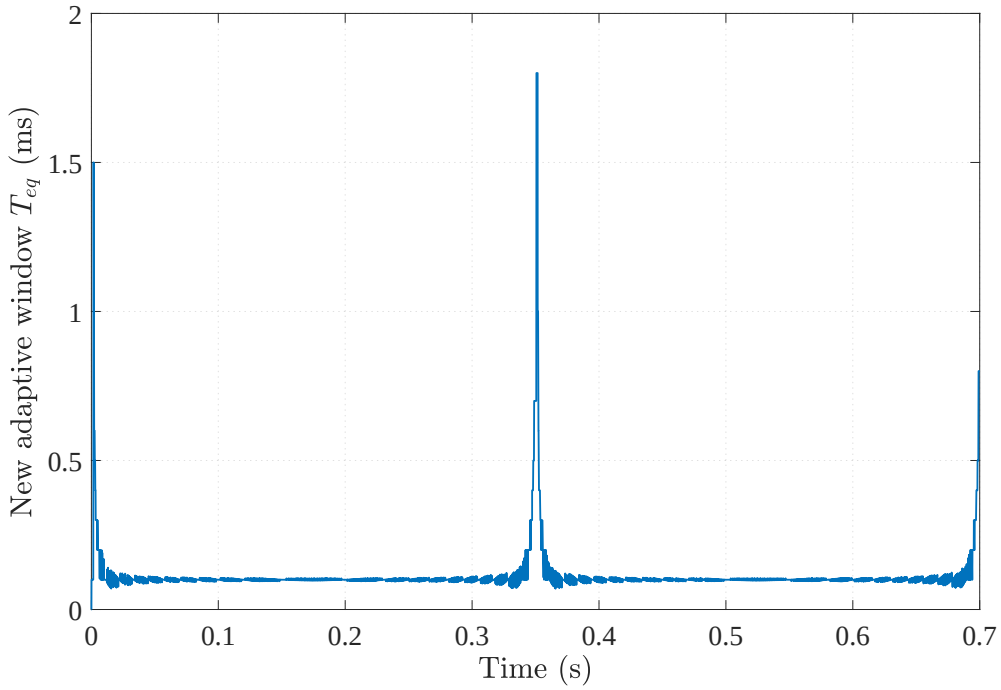

Figure 4.16: Pulse-window synchronization method: new observation window plot for $T_w = 0.1$ ms, $T_h = 0.1$ μs, $N_{pr} = 2048$ ppr, and $\omega_r(\mathrm{max}) = 3000$ rpm.

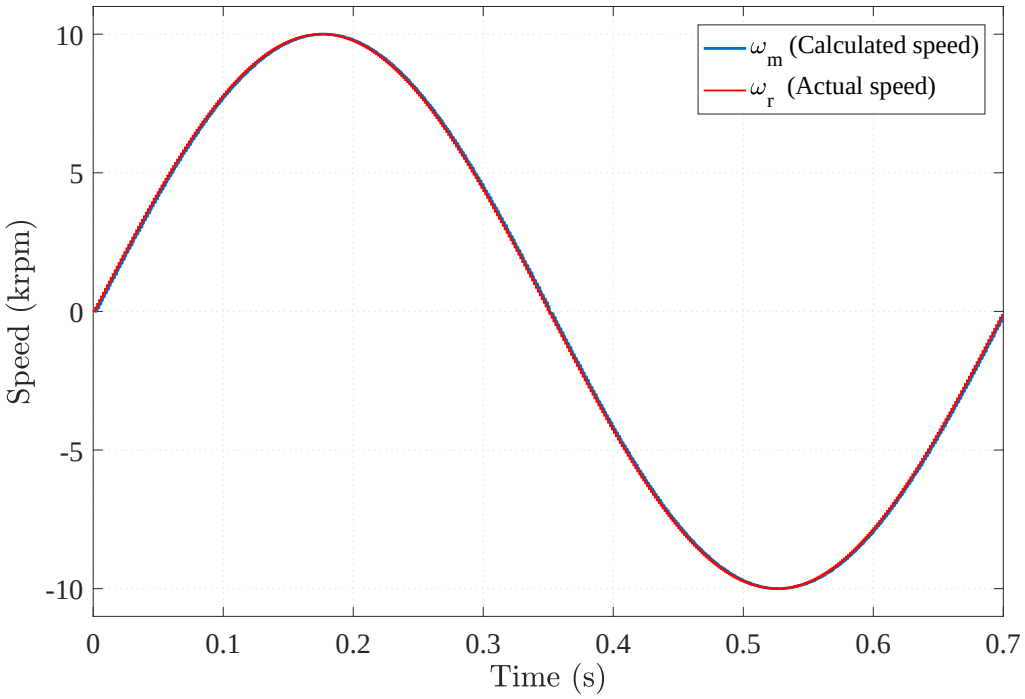

Figure 4.17: Pulse-window synchronization method: speed response for T_w = 1.5 ms, T_h = 0.1 μs, N_{pr} = 4000 ppr.

seems good with these parameters. Now, if we change the basic time window to T_w = 0.15 ms, the response shows some fluctuations in speed calculation which is due to the quantization error introduced by time window calculation. It is shown in Fig. 4.18.

In order to examine the behavior of pulse-window synchronization method in low speed range, a simulation is performed for T_w = 10 ms, T_h = 0.1 μs, N_{pr} = 590 ppr and $\omega_{\mathrm{r}}(\mathrm{max})$ = 195 rpm. Fig. 4.19 shows that calculated speed is almost similar to the sampled version of input signal with one step computational delay. The basic time window width is chosen in order to get some encoder pulses in it. Fig. 4.20 presents the speed response for the basic time window of 5 ms. The small fluctuations in the calculated speed response are now prominent with the reduced time window.

The pulse-window synchronization method seems good in all speed range without any need for switching like in the combined method (frequency and period measurement method). The only issue is to select the proper sampling of data required for the speed calculation. The accuracy of this method is affected only by the period measurement of the basic time window and is comparable with the period measurement method in the low speed region. The accuracy is higher in high speed region and is limited only when the high frequency clock signal used for the period measurements becomes comparable with encoder pulse signals. The corresponding quantization error then becomes non-negligible.

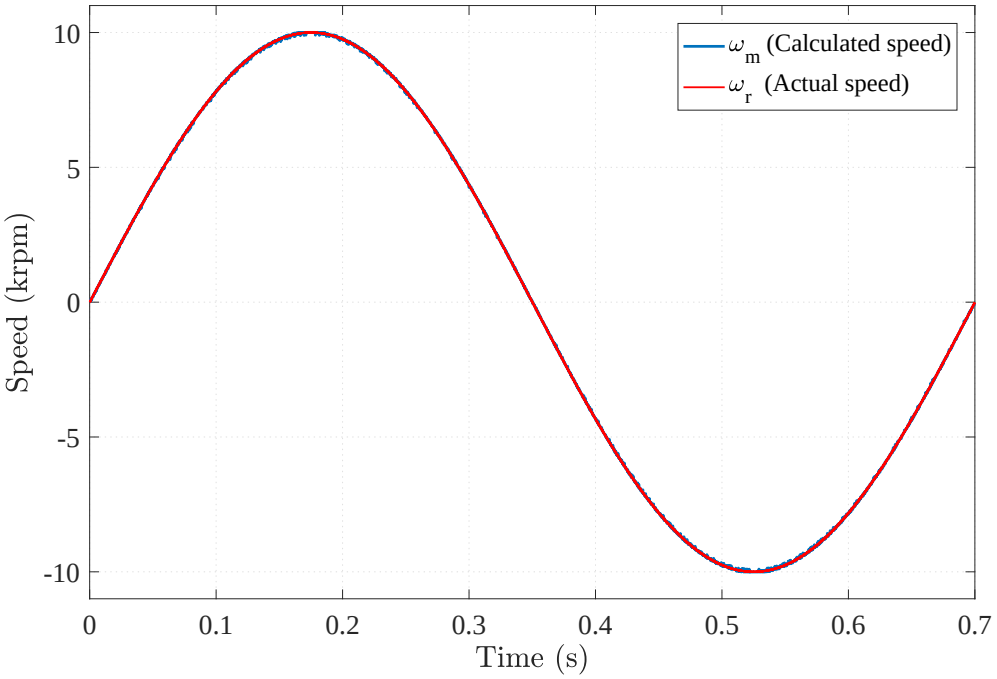

Figure 4.18: Pulse-window synchronization method: speed response for $T_w = 0.15$ ms, $T_h = 0.1$ μs, $N_{pr} = 4000$ ppr.

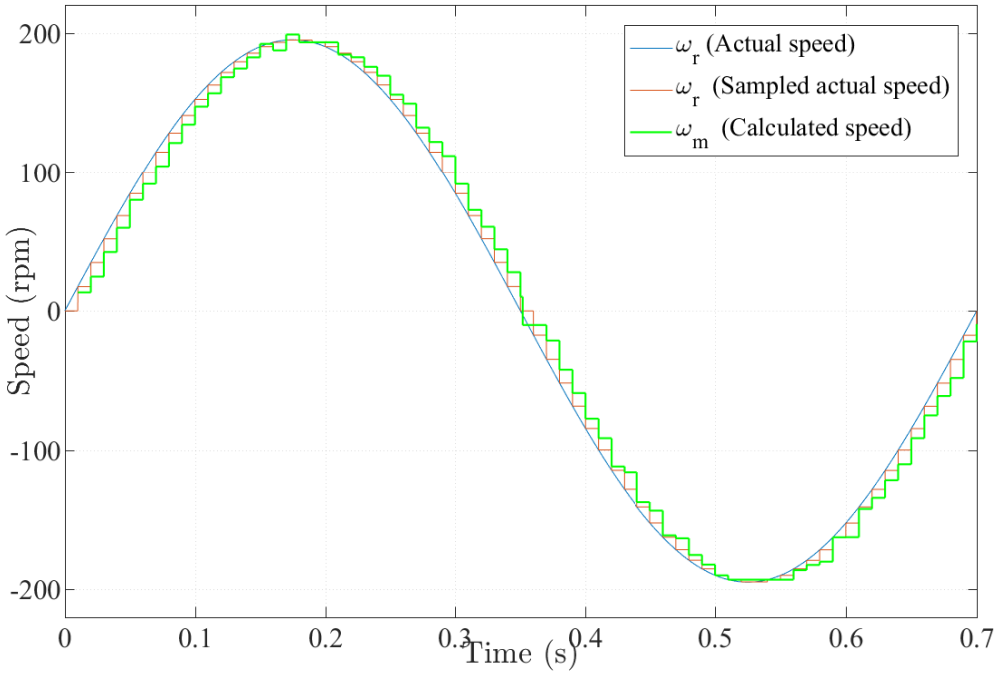

Figure 4.19: Pulse-window synchronization method: speed response for $T_w = 10$ ms, $T_h = 0.1$ μs, $N_{pr} = 590$ ppr.

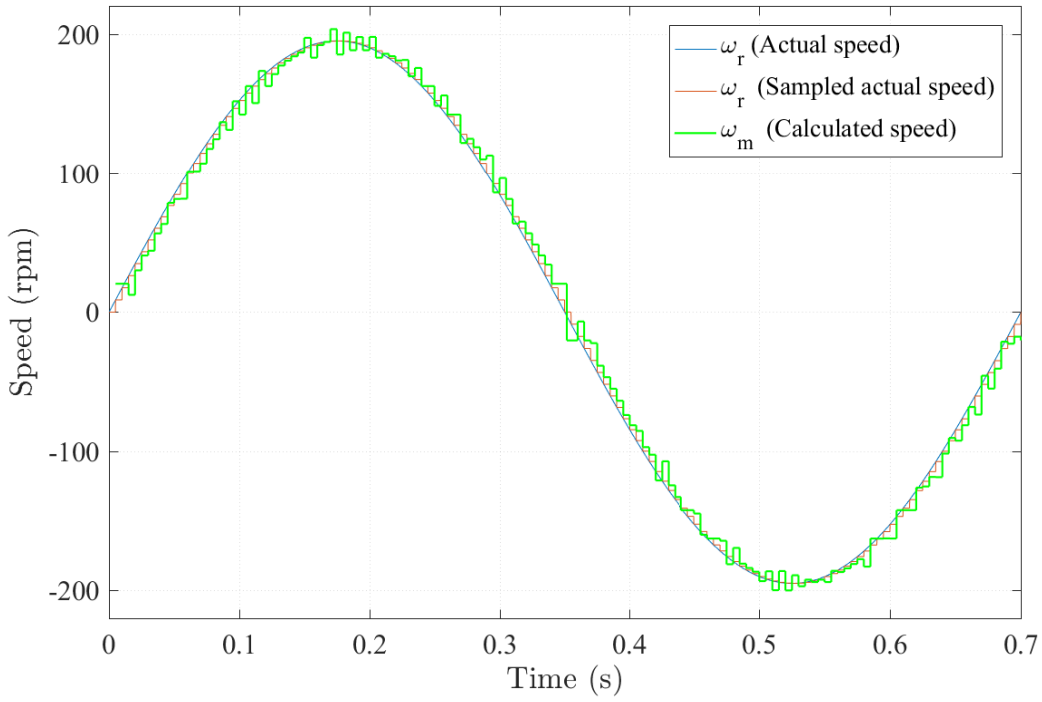

Figure 4.20: Pulse-window synchronization method: speed response for $T_w = 5$ ms, $T_h = 0.1$ μs, $N_{pr} = 590$ ppr.

4.5 Comparison summary

Table 4.1: Comparison summary for the speed decoding algorithms based on the simulation results.

Speed decoding methods	Normal speed operation with typical encoder resolution (e.g. $\omega_r = 3000$ rpm, $N_{pr} = 2048$ ppr)	High speed operation with high encoder resolution (e.g. $\omega_r = 10000$ rpm, $N_{pr} = 4000$ ppr)	Low speed operation with low resolution encoder (e.g. $\omega_r = 200$ rpm, $N_{pr} = 590$ ppr)	Remarks
Frequency Measurement Method	- Moderate - Accuracy increases with the speed	- Very high accuracy at high speeds	- High quantization error - Poor accuracy	- Most suitable for high speed range applications - Simple and classical method
Period Measurement Method	- Moderate - Accuracy decreases with increase in the speed	- Accuracy suffers at high speeds - High quantization error at higher speeds	- Moderate - High accuracy	- Most suitable for low speed range applications - Simple structure
Combined Method	- Moderate - High accuracy	- Moderate - High accuracy	- Moderate - High accuracy	- Suitable for wide speed range - Quantization error still present - Switching mechanism required - Straightforward implementation
Pulse-window synchronization method	- Moderate - High accuracy	- Moderate - High accuracy	- Moderate - High accuracy	- Suitable for wide speed range application - Quantization error due to period measurement counters - Correct sampling of data is required - Complex implementation

A comparison summary for the implemented speed decoding algorithms is presented in Table 4.1 based on simulation results. The summary shows that both the combined and pulse-window synchronization methods are applicable to wide speed range. The combined method for speed computation requires a sophisticated switching mechanism with minimum time duration. The accuracy is improved but quantization error still exists. On the other hand, the pulse-window synchronization method provides excellent results in all speed ranges. It removes the quantization error problem due to lack of synchronization between basic time window and encoder pulses. Moreover, it does not involve the need for a switching mechanism. The only quantization error in this method is introduced during the period measurement process by high frequency counters. However, the main implementation problem is to get the correct sampling of data needed for speed calculation. The pulse-window synchronization method is selected and implementation is done in Xilinx FPGA based on the results.

5 Implementation of pulse-window synchronization

In this Section, the pulse-window synchronization algorithm is implemented in Xilinx FPGA. The implemented algorithm is simulated in various speed regions with different values of encoder resolution and the results are analyzed.

5.1 Results

The pulse-window synchronization method for speed calculation is implemented and analyzed under different situations. The FPGA model based speed response in normal speed range ($\leq$ 3000 rpm) with encoder resolution of 2048 ppr is shown in Fig. 5.1. The basic time window was set at $T_w = 1.5$ ms and high frequency clock pulse time period was $T_h = 0.1$ μs required for period measurements. The resulted

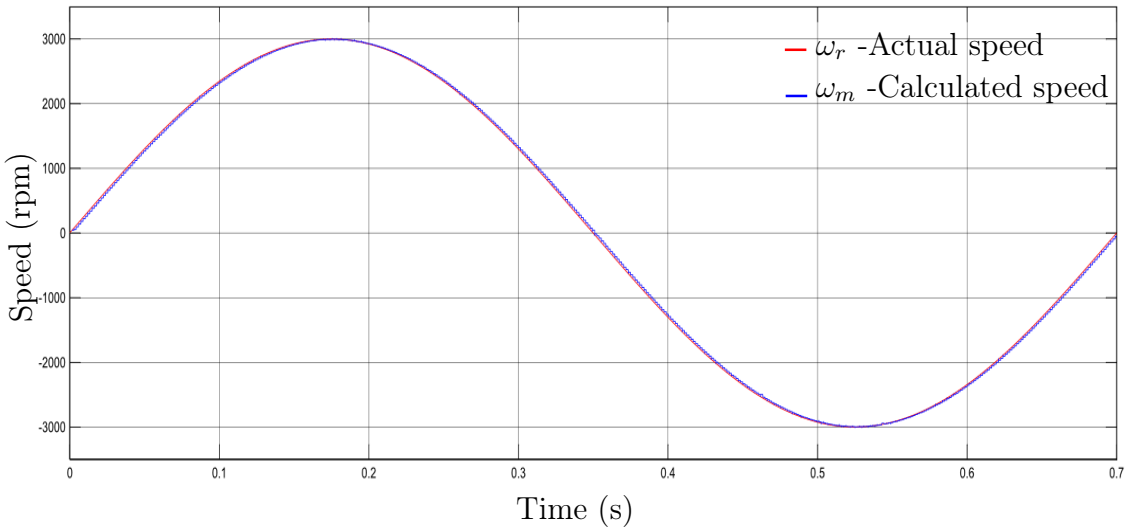

Figure 5.1: Speed response for $T_w = 1.5$ ms, $T_h = 0.1$ μs, and $N_{pr} = 2048$.

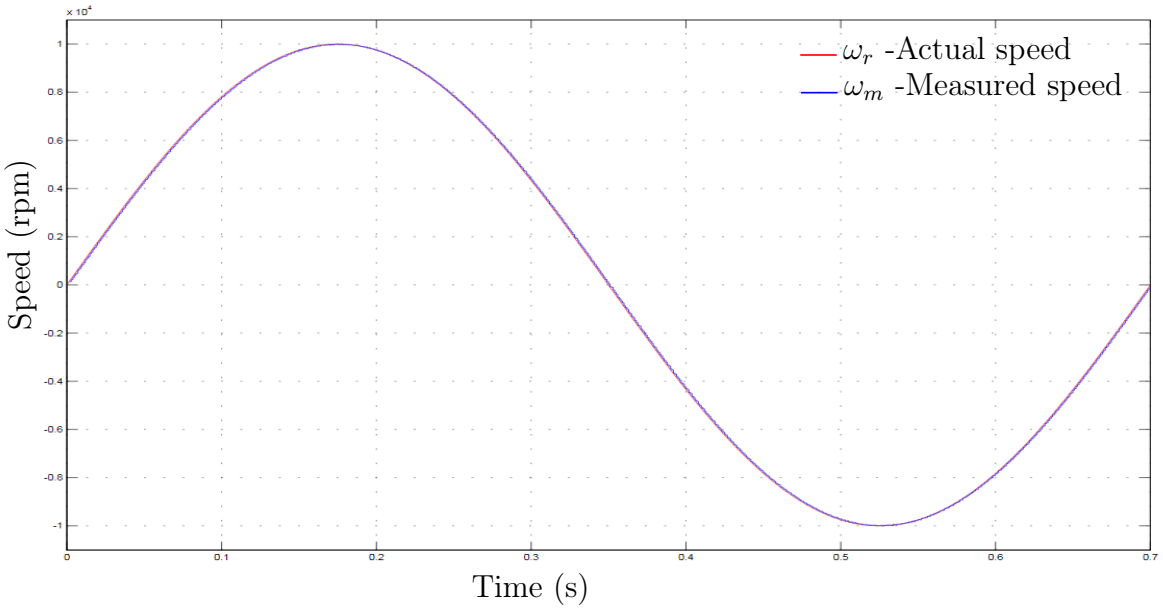

Figure 5.2: Speed response for T_w = 1 ms, T_h = 0.1 μs, and N_{pr} = 4000.

speed response shows that the calculated speed follows the actual speed signal well. The speed response to a sinusoidal input signal of amplitude 10000 rpm and high resolution incremental encoder (N_{pr} = 4000 ppr) is shown in Fig. 5.2.

The basic time window is set at T_w = 1 ms while T_h = 0.1 μs. The result shows that the pulse-window synchronization method can be perfectly suitable for the high speed applications. Further, the pulse-window synchronization method was analyzed in the low speed region with the low resolution incremental encoder.

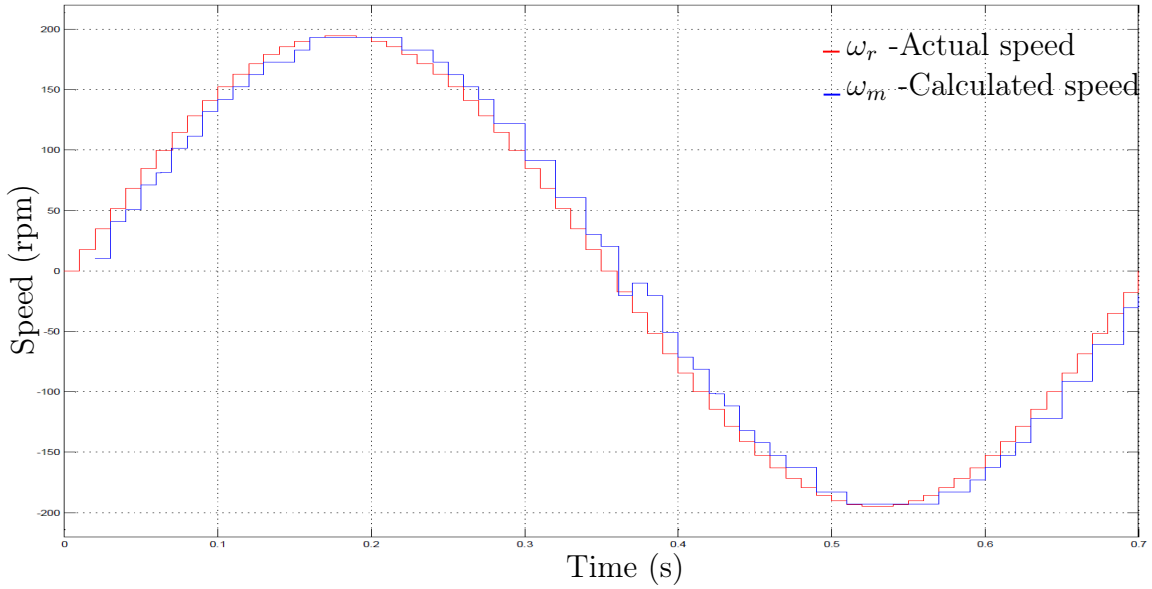

Figure 5.3: Speed response for T_w = 10 ms, T_h = 0.1 μs, and N_{pr} = 590.

The resolution of the incremental encoder was set at 590 rpm with input sinusoidal speed input of amplitude 195 rpm. For $T_w = 10$ ms, and $T_h = 0.1$ μs the resulted speed response is shown in Fig. 5.3. Both the reference and calculated speed signals are sampled at $T_s = 10$ ms. Based on results, it can be noticed that the pulse-window synchronization method is applicable to all speed range applications. There is no need to change from one speed decoding method to another. The quantization error problem as discussed in frequency measurement method is removed by this algorithm.

6 Conclusion

In this thesis, the state-of-the-art speed decoding algorithms are presented for rotary incremental encoders. Each algorithm is investigated by literature review. Various types of incremental encoders are also discussed based on their design structure and operating principle. Each of the speed decoding algorithm along with an incremental encoder is implemented in Matlab Simulink in order to further investigate the behavior. The effect of incremental encoder resolution is also analysed. The speed response of each algorithm is examined in low, normal and high speed regions. The final results are analysed and a comparative analysis is done based on accuracy, rapid response time and wide speed applications. A best approach for speed calculation is selected and implemented in Xilinx FPGA.

The results show that the frequency measurement method for speed calculation is the most suitable choice for high speed applications only. It gives high relative error at low speeds which decreases when the number of encoder pulses inside time observation window increases. On the other hand, the relative error in period measurement method is high at high speeds. The period measurement method has high accuracy in low speed regions than frequency measurement method. However, none of them is a suitable choice for a wide speed range. The combined method performs well in a wide speed range and combines the advantages of both frequency and period measurement methods. It compares the relative error for both methods and based on that switches to the best approach with low relative error. The quantization error problem is still present due to lack of synchronization of time observation window and encoder pulses. In pulse-window synchronization method for speed computation, the encoder pulses are synchronized with observation window and corresponding quantization error reduces to zero. The pulse-window synchronization method removes the quantization error without using a switching mechanism. The only quantization error is introduced during the period measurement process by high frequency counters. The main disadvantage of pulse-window synchronization

method is the correct sampling of data required for speed computation. Both the combined method and pulse-window synchronization method for speed calculation can be used for wide speed applications. The pulse-window synchronization method is implemented in Xilinx FPGA since it has no switching mechanism and quantization error due to lack of synchronization between observation window and encoder pulse is zero. The simulations are performed in high, low and conventional speed regions and results are verified.

Overall, the objectives of this thesis are achieved. Based on results a comparative analysis shows that the combined method and pulse-window synchronization can be the most suitable choice for a wide speed range. However, each of these methods has its own limitations. In pulse-window synchronization method there is a need to solve the problem of the correct sampling of data which is required to calculate speed. Pulse-window synchronization method is difficult to implement in comparison with combined method. On the other hand, combined method only limits the quantization error due to lack of synchronization between encoder pulses and time window, but does not completely remove it. In future, further developments are needed to solve these issues in both methods to get more accurate results.

References

[1] R. M. Kennel, "Why do incremental encoders do a reasonably good job in electrical drives with digital control?" in *Conference Record of the 2006 IEEE Industry Applications Conference Forty-First IAS Annual Meeting*, vol. 2, Oct 2006, pp. 925–930.

[2] F. Briz, J. A. Cancelas, and A. Diez, "Speed measurement using rotary encoders for high performance ac drives," in *Industrial Electronics, Control and Instrumentation, (IECON) '94*, vol. 1, Sept. 1994, pp. 538–542.

[3] R. Petrella, M. Tursini, L. Peretti, and M. Zigliotto, "Speed measurement algorithms for low-resolution incremental encoder equipped drives: a comparative analysis," in *Electrical Machines and Power Electronics, (ACEMP)*, Sept. 2007, pp. 780–787.

[4] R. D. Lorenz and K. V. Patten, "High resolution velocity estimation for all digital, ac servo drives," in *Conference Record of the 1988 IEEE Industry Applications Society Annual Meeting*, Oct 1988, pp. 363–368 vol.1.

[5] H. Wang and J.-t. Pu, *An Improved Variable M/T Method Based on Speed Estimation for Optical Incremental Encoders.* Berlin, Heidelberg: Springer Berlin Heidelberg, 2013, pp. 13–20. [Online]. Available: http://dx.doi.org/10.1007/978-3-642-33012-4_2

[6] I. I. Incze, C. Szabó, and M. Imecs, *Incremental Encoder in Electrical Drives: Modeling and Simulation.* Berlin, Heidelberg: Springer Berlin Heidelberg, 2010, pp. 287–300. [Online]. Available: http://dx.doi.org/10.1007/978-3-642-15220-7_23

[7] J. J. Incze, C. Szabó, and M. Imecs, "Modeling and simulation of an incremental encoder used in electrical drives," in *Proceedings of 10th International Symposium of Hungarian Researchers on Computational Intelligence and Informatics, Budapest, Hungary, November*, 2009, pp. 12–14.

[8] T. Ohmae, T. Matsuda, K. Kamiyama, and M. Tachikawa, "A microprocessor-controlled high-accuracy wide-range speed regulator for motor drives," *IEEE Transactions on Industrial Electronics*, vol. IE-29, no. 3, pp. 207–211, Aug. 1982.

[9] O. Baser, E. Kilic, E. I. Konukseven, and M. Dolen, "A hybrid method to estimate velocity and acceleration using low-resolution optical incremental encoders," in *Signals and Electronic Systems, (ICSES)*, Sept. 2010, pp. 57–60.

[10] N. Stojkovic, Z. Stare, and N. Mijat, "Dual-mode digital revolution counter," in *IMTC 2001. Proceedings of the 18th IEEE Instrumentation and Measurement Technology Conference. Rediscovering Measurement in the Age of Informatics (Cat. No.01CH 37188)*, vol. 2, 2001, pp. 950–954 vol.2.

[11] T. Tsuji, T. Hashimoto, H. Kobayashi, M. Mizuochi, and K. Ohnishi, "A wide-range velocity measurement method for motion control," *IEEE Transactions on Industrial Electronics*, vol. 56, no. 2, pp. 510–519, Feb. 2009.

[12] R. Petrella and M. Tursini, "An embedded system for position and speed measurement adopting incremental encoders," *IEEE Transactions on Industry Applications*, vol. 44, no. 5, pp. 1436–1444, Sept. 2008.

[13] L. D. Cintio, F. Parasiliti, R. Petrella, and M. Tursini, "A novel approach to speed measurement for incremental encoders featuring high accuracy and bandwidth," *Proc. of 11th EPE-PEMC*, Sep. 2-4 2004, CD-ROM.

[14] C. W. de Silva, *Sensors and Actuators: Engineering System Instrumentation.* Taylor & Francis Group: CRC Press, 2016.

[15] B. Drury, *Control Techniques Drives and Controls Handbook (2nd Edition).* Institution of Engineering and Technology, 2009. [Online]. Available: http://app.knovel.com/hotlink/toc/id:kpCTDCHE08/control-techniques-drives/control-techniques-drives

[16] R. M. Jens Weidauer, *Electrical Drives: Principles, Planning, Applications, Solutions.* Publicis Publishing, 2014.

[17] J. G. Webster, *The Measurement, Instrumentation and Sensors Handbook.* Taylor & Francis Group: CRC Press, 2014.

[18] R. Crowder, *Electric Drives and Electromechanical Systems: Applications and Control.* Elsevier, 2006.

[19] J. Jacobs, *Incremental & Absolute Encoders: What's the Best Solution for Your Application?*, DYNAPAR. [Online]. Available: http://www.dynapar.com/uploadedFiles/_Site_Root/Technology/White_Papers/New_incremental%20absolute_7_29_13.pdf

[20] D. S. Nyce, *ENCODERS.* John Wiley & Sons, Inc., 2016, pp. 315–333. [Online]. Available: http://dx.doi.org/10.1002/9781119069164.ch13

[21] R. Siegwart, I. R. Nourbakhsh, and D. Scaramuzza, *Introduction to Autonomous Mobile Robots*, 2nd ed. The MIT Press, 2011.

[22] LEINE & LINDE, "Heavy Duty 800 Series: Incremental encoders for heavy duty industries." [Online]. Available: http://www.leinelinde.com/products/heavy-duty-encoders/800-heavy-duty/

[23] R. C. Kavanagh, "Improved digital tachometer with reduced sensitivity to sensor nonideality," *IEEE Transactions on Industrial Electronics*, vol. 47, no. 4, pp. 890–897, Aug. 2000.